Local discontinuous Galerkin methods for the carpet cloak model

Xinyue Yu, * Jichun Li, † Chi-Wang Shu ‡

January 30, 2022

Abstract.

The DG methods have been shown to have good performance in numerical simulations of the carpet cloak model in [32]. However, the stability analysis and the error estimate are left to be done. In this paper, we introduce the leap-frog DG methods to solve the carpet cloak model. We prove the stability of the semi-discrete scheme, the sub-optimal error estimate for unstructured meshes, and the optimal error estimate for tensor-product meshes. Then, the fully discrete scheme is stated and the stability is proved. Finally, the numerical accuracy tests on rectangular and triangular meshes are given respectively, and the results of numerical simulations of the wave propagation in the carpet cloak model using the DG scheme are presented.

Keywords – Discontinuous Galerkin method, Maxwell's equations, metamaterials, leap-frog scheme.

1 Introduction

Since Leonhardt [26] and Pendry *et al.* [40] firstly demonstrated the idea of invisibility cloak design with metamaterials in 2006, much study has been done in both theoretical and numerical analysis. There are a plenty of excellent works on the mathematical analysis of the cloaking phenomenon [1, 23, 17, 18], and on the numerical simulations of the cloaking models with the finite different (FD) methods [19, 22, 36], the finite element (FE) methods [4, 25, 30, 39], and the spectral methods [46, 47]. For more details, readers can consult the review papers [2, 6, 21], and the monographs [15, 20, 29, 38] as references. In 2014, Li *et al.* proposed the mathematical analysis for the time-domain carpet cloak model [30]. In [32], a revised finite difference method for the carpet cloak model was developed, and the corresponding stability analysis was performed with the time step constraint $\tau = O(h^2)$, where τ and h are the time step size and spatial mesh size respectively. In order to relax the time step constraint to $\tau = O(h)$, the usual requirement for the FD or the FE methods to solve the time-dependent Maxwell equations, a new energy was introduced in [34]; moreover, the finite element method coupled with two time discretization methods to solve the carpet cloak model was developed therein.

The discontinuous Galerkin (DG) method was initially proposed by Reed and Hill [42] to solve the neutron transport problem. Later, Cockburn and Shu introduced the Runge-Kutta DG (RKDG)

*Division of Applied Mathematics, Brown University, Providence, RI 02912, USA. (xinyue_yu@brown.edu)

†Department of Mathematical Sciences, University of Nevada Las Vegas, Las Vegas, Nevada 89154-4020, USA. (jichun.li@unlv.edu). Research supported by NSF grant DMS-2011943.

‡Division of Applied Mathematics, Brown University, Providence, RI 02912, USA. (chi-wang_shu@brown.edu). Research supported by AFOSR grant FA9550-20-1-0055 and NSF grant DMS-2010107.

methods for solving the linear and nonlinear hyperbolic partial differential equations (PDEs) [11, 12], and the local DG (LDG) methods for solving the time-dependent convection-diffusion systems [13], which stimulated the rapid development and application of the DG methods [14, 45]. The DG method shares the advantages of the continuous finite element methods, including flexible h-p adaptivity and easy handling of the complicated geometry. Additionally, it has unique nice features, such as it has the local mass matrix because of the discontinuous basis, it allows easy handling of hanging nodes and adaptivity, and it has high parallel efficiency. Attracted by the good properties of the DG methods, mathematicians have developed the DG methods to solve the Maxwell equations in free space [5, 7, 10, 16, 44], and in dispersive media [24, 37, 44]. For the Maxwell equations in the metamaterials, there are published works on the DG methods to solve the Drude models [27, 28, 33, 35, 43], the Maxwell equations in nonlinear optical media [3], and the wave propagation in media with dielectrics and metamaterials [8].

In [32], the DG method was carried out to solve the carpet cloak model, and it gave a good performance in numerical simulations. However, the stability analysis and the error estimate of the method were left to be done. This paper is a follow up of [32], and the rest of the paper is organized as follows. In Sect. 2, the governing equations for the carpet cloak model are presented. In Sect. 3, we propose the semi-discrete DG method for the model, and prove its stability. Next, we provide a sub-optimal error estimate in the L^2 norm on unstructured meshes, and an optimal error estimate on tensor-product rectangular meshes. Then, a fully discrete DG method with the leap-frog time discretization is presented in sect. 4, followed by the corresponding stability analysis. Sect. 5 shows several numerical experiments, including the accuracy tests for the proposed DG method. Additionally, the wave propagation simulations in the carpet cloak region are also demonstrated in this section. Finally, we give the concluding remarks in Sect. 6.

2 The governing equations

The governing equations for modeling the wave propagation in the carpet cloak are derived in [31] and given as follows (cf. [31, (2.3)-(2.5)]):

$$\partial_t D_x = \frac{\partial H}{\partial y}, \tag{1}$$

$$\partial_t D_y = -\frac{\partial H}{\partial x}, \tag{2}$$

$$\varepsilon_0 \lambda_2 \left(M_A^{-1} \partial_{t^2} \boldsymbol{E} + \omega_p^2 M_A^{-1} \boldsymbol{E} \right) = \partial_{t^2} \boldsymbol{D} + M_C \boldsymbol{D}, \tag{3}$$

$$\mu_0 \mu \partial_t H = -\nabla \times \boldsymbol{E}, \tag{4}$$

where we denote $\boldsymbol{D} := (D_x, D_y)'$ for the 2D electric displacement, $\boldsymbol{E} := (E_x, E_y)'$ for the 2D electric field, and H for the magnetic field. Furthermore, we denote $\partial_{t^k} u$ for the k-th derivative $\partial^k u / \partial t^k$ of a function u. For any $k \geq 1$, we adopt the 2D vector and scalar curl operators:

$$\nabla \times H = (\frac{\partial H}{\partial y}, -\frac{\partial H}{\partial x})', \quad \nabla \times \boldsymbol{E} = \frac{\partial E_y}{\partial x} - \frac{\partial E_x}{\partial y}, \quad \forall\ \boldsymbol{E} = (E_x, E_y)'.$$

Note that (3) is revised from [31, (2.4)] by left-multiplying both sides with M_A^{-1} and by denoting matrix $M_C = M_A^{-1} M_B$. Here we denote M_A^{-1} as the inverse of the matrix M_A, which is proved to be symmetric positive definite [31, Lemma 2.1]. As shown in Fig. 1, the governing equations (1)-(4)

hold true in the cloaking region formed by the quadrilateral with vertices $(-d,0),(0,H_1),(d,0)$ and $(0,H_2)$, where d,H_1 and H_2 are positive constants and $H_2 > H_1 > 0$. The cloaked region, where the hiding objects can be placed, is formed by the triangle with vertices $(0,H_1),(-d,0)$ and $(d,0)$.

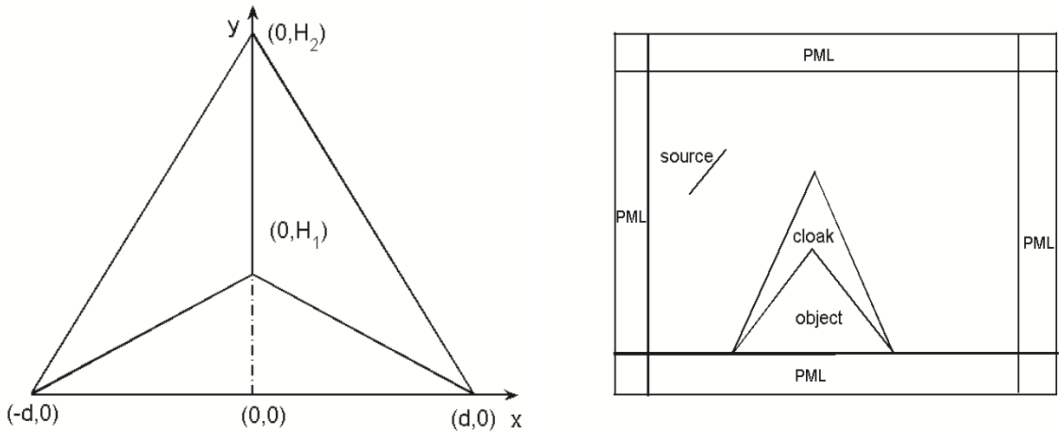

Figure 1: Left: The structure of the carpet cloak. Right: The setup of the carpet cloak simulation.

In order to make those objects inside the cloaked region invisible, the permittivity and permeability in the cloaking region need to be specially designed and are given by [31]:

$$\varepsilon = \begin{bmatrix} a & b \\ b & c \end{bmatrix} := \begin{bmatrix} \frac{H_2}{H_2-H_1} & -\frac{H_1H_2}{(H_2-H_1)d}\mathrm{sgn}(x) \\ -\frac{H_1H_2}{(H_2-H_1)d}\mathrm{sgn}(x) & \frac{H_2-H_1}{H_2} + \frac{H_2}{H_2-H_1}(\frac{H_1}{d})^2 \end{bmatrix}, \quad \mu = a,$$

where $\mathrm{sgn}(x)$ denotes the sign function. Furthermore, in (1)-(3), the ε_0 and μ_0 denote the permittivity and permeability in free space, respectively; the matrices M_A and M_B are given as [31, p.1138]:

$$M_A = \begin{pmatrix} p_1^2\lambda_2 + p_2^2 & p_2p_4 + p_1p_3\lambda_2 \\ p_2p_4 + p_1p_3\lambda_2 & p_3^2\lambda_2 + p_4^2 \end{pmatrix}, \quad M_B = \begin{pmatrix} p_2^2 & p_2p_4 \\ p_2p_4 & p_4^2 \end{pmatrix}\omega_p^2,$$

where the positive constant ω_p is the plasma frequency resulting from the Drude dispersion model [31, p.1138], elements $p_i, i = 1,2,3,4$, are

$$p_1 = \sqrt{\frac{\lambda_2 - a}{\lambda_2 - \lambda_1}},\ p_2 = -\sqrt{\frac{a - \lambda_1}{\lambda_2 - \lambda_1}} \cdot \mathrm{sgn}(x),\ p_3 = \sqrt{\frac{\lambda_2 - c}{\lambda_2 - \lambda_1}} \cdot \mathrm{sgn}(x),\ p_4 = \sqrt{\frac{c - \lambda_1}{\lambda_2 - \lambda_1}},$$

and λ_1 and λ_2 are the eigenvalues of matrix ε given as:

$$\lambda_1 = \frac{a + c - \sqrt{(a-c)^2 + 4b^2}}{2}, \quad \lambda_2 = \frac{a + c + \sqrt{(a-c)^2 + 4b^2}}{2}.$$

To complete the carpet cloak model (1)-(4), we assume that (1)-(4) satisfy the initial conditions

$$\begin{aligned} &\boldsymbol{D}(\boldsymbol{x},0) = \boldsymbol{D}_0(\boldsymbol{x}), \quad \boldsymbol{E}(\boldsymbol{x},0) = \boldsymbol{E}_0(\boldsymbol{x}), \quad H(\boldsymbol{x},0) = H_0(\boldsymbol{x}), \\ &\partial_t\boldsymbol{D}(\boldsymbol{x},0) = \boldsymbol{D}_1(\boldsymbol{x}), \quad \partial_t\boldsymbol{E}(\boldsymbol{x},0) = \boldsymbol{E}_1(\boldsymbol{x}), \quad \forall\ \boldsymbol{x} \in\ \Omega, \end{aligned} \tag{5}$$

and the perfect conducting boundary condition (PEC):

$$\boldsymbol{n} \times \boldsymbol{E} = \boldsymbol{0} \quad \text{on } \partial\Omega, \tag{6}$$

where $\boldsymbol{D}_0, \boldsymbol{D}_1, \boldsymbol{E}_0, \boldsymbol{E}_1$ and H_0 are some properly given functions, $\boldsymbol{n}$ is the unit outward normal vector to $\partial\Omega$, and Ω denotes a polygonal domain in R^2.

Using the stability obtained in [34, Theorem 2.1] and replacing both $\nabla \times \boldsymbol{E}$ and $\nabla \times \partial_t \boldsymbol{E}$ by (4), we can rewrite Theorem 2.1 of [34] as below, which is totally different from those established in [31, 32].

Theorem 2.1. *For the solution $(\boldsymbol{D}, H, \boldsymbol{E})$ of (1)-(4), denote the energy*

$$\begin{aligned} ENG(t) \;:=\; & \Big[\varepsilon_0\lambda_2||M_A^{-\frac{1}{2}}\partial_{t^2}\boldsymbol{E}||^2 + 2\varepsilon_0\lambda_2\omega_p^2||M_A^{-\frac{1}{2}}\partial_t\boldsymbol{E}||^2 + \varepsilon_0\lambda_2\omega_p^4||M_A^{-\frac{1}{2}}\boldsymbol{E}||^2 \\ & +\mu_0\mu\left(\omega_p^2||\partial_t H||^2 + ||\partial_{t^2} H||^2\right) + ||\partial_t\boldsymbol{D}||^2 + ||M_C^{\frac{1}{2}}\boldsymbol{D}||^2\Big](t). \end{aligned} \tag{7}$$

Here and below we denote $M_C^{\frac{1}{2}}$ for the square root of a matrix M_C, and $||\cdot||^2 := ||\cdot||^2_{L^2(\Omega)}$. Then we have the following energy identity:

$$\begin{aligned} & ENG(t) - ENG(0) \\ = \;& 2\int_0^t \left[\varepsilon_0\lambda_2(M_A^{-1}\partial_{t^2}\boldsymbol{E} + \omega_p^2 M_A^{-1}\boldsymbol{E}, \partial_t\boldsymbol{D}) + (M_C\partial_t\boldsymbol{D}, \partial_{t^2}\boldsymbol{E}) + \omega_p^2(M_C\boldsymbol{D}, \partial_t\boldsymbol{E})\right] dt. \end{aligned} \tag{8}$$

Furthermore, this leads to the stability:

$$ENG(t) \le ENG(0) \cdot \exp(C_* t), \quad \forall\ t \in [0, T], \tag{9}$$

where the constant $C_* > 0$ depends on the physical parameters $\varepsilon_0, \mu_0, d, H_1, H_2$ and ω_p.

3 The semi-discrete LDG method

In this section, we introduce the LDG method for the carpet cloak model. We consider a rectangular physical domain $\Omega = [a, b] \times [c, d]$ to solve (1)-(4) for simplicity, and the domain is partitioned by a regular triangular mesh, $\Omega = \cup_{e\in\mathcal{T}_h} e$. Here $\mathcal{T}_h$ is a triangulation on Ω, and h is the mesh size, representing the largest diameter of all triangles. Tensor-product rectangular meshes will also be considered later. The time domain $[0, T]$ is discretized into $N_t + 1$ uniform intervals by discrete times $0 = t_0 < t_1 < \cdots < t_{N_t+1} = T$, where $t_n = n \cdot \tau$, and the time step size $\tau = \frac{T}{N_t+1}$.

We denote V_h^k as the finite element space of piecewise polynomials, i.e.,

$$V_h^k = \{v :\ v|_e \in P_k(e), \quad \forall\ e \in \mathcal{T}_h\}, \tag{10}$$

where P_k is the space of polynomials of degree less or equal to k.

We denote u_h as the corresponding numerical solution of the variable u, which is in the finite element space V_h^k. Note that functions contained in V_h^k can have discontinuities across the element interfaces. In the line integral over the boundary of a cell, we denote $u_h^{(in)}$ as the value of u_h taken

from inside of that cell, and $u_h^{(out)}$ from the neighboring cell sharing that boundary. Furthermore, $(\cdot)$ and $||\cdot||$ are denoted as the inner product and the L^2 norm over the domain Ω respectively.

Then, the semi-discrete LDG method for (1)-(4) is generated as follows: Find $E_{xh}, E_{yh}, H_h, D_{xh}, D_{yh} \in C^1([0,T]; V_h^k)$ such that

$$\int_e \partial_t D_{xh}\phi_x + \int_e H_h \partial_y \phi_x - \int_{\partial e} \hat{H}_h \phi_x^{(\text{in})} n_y^{(in)} = 0, \tag{11}$$

$$\int_e \partial_t D_{yh}\phi_y - \int_e H_h \partial_x \phi_y + \int_{\partial e} \hat{H}_h \phi_y^{(\text{in})} n_x^{(in)} = 0, \tag{12}$$

$$\varepsilon_0\lambda_2 \int_e \left(M_A^{-1}\partial_{t^2}\boldsymbol{E}_h + \omega_p^2 M_A^{-1}\boldsymbol{E}_h\right)\cdot\boldsymbol{u} = \int_e (\partial_{t^2}\boldsymbol{D}_h + M_C\boldsymbol{D}_h)\cdot\boldsymbol{u}, \tag{13}$$

$$\mu_0\mu \int_e \partial_t H_h\psi - \int_e E_{yh}\partial_x\psi + \int_e E_{xh}\partial_y\psi + \int_{\partial e}(\hat{E}_{yh}n_x^{(in)} - \hat{E}_{xh}n_y^{(in)})\psi^{(\text{in})} = 0, \tag{14}$$

for all test functions $\phi_x, \phi_y, \psi, u_1, u_2 \in V_h^k$ and all triangle cells $e \in \mathcal{T}_h$, where $\boldsymbol{u} = (u_1, u_2)'$. $\hat{H}_h, \hat{E}_{yh}, \hat{E}_{xh}$ are the cell boundary terms obtained from integration by parts, and they are the so-called numerical fluxes. On the cell boundary ∂e, $\boldsymbol{n}^{(in)} = (n_x^{(in)}, n_y^{(in)})$ represents the unit normal vector pointing towards the outside of the element e.

To define the numerical fluxes in a triangulation, we firstly pick a fix direction $\boldsymbol{\beta}$ not parallel to any triangle boundary edge. On each boundary edge of an element, there is an outward normal direction, $\boldsymbol{n}$, orthogonal to that edge. We call a side as the "right" side if $\boldsymbol{n}\cdot\boldsymbol{\beta} < 0$, and the "left" side if vice versa. We apply the commonly used alternating fluxes in LDG methods into our scheme, which are defined as choosing E_{xh} and E_{yh} on the "right" side and H_{zh} on the "left" side:

$$\hat{E}_{xh} = E_{xh}^R, \tag{15}$$

$$\hat{E}_{yh} = E_{yh}^R, \tag{16}$$

$$\hat{H}_h = H_h^L. \tag{17}$$

A more detailed explanation of alternating fluxes for triangulations can be found in [45]. It is easy to check that in a rectangular mesh, when $\boldsymbol{\beta} = (1,1)$, the definitions of the "left" and "right" sides are consistent with the exact left (bottom) and right (top) sides on a vertical (horizontal) boundary. The above definition of alternating fluxes is enough when applying the periodic boundary condition. However, to satisfy the PEC boundary condition in (6), we take

$$\hat{E}_{xh} = 0, \text{ on } y = c, d, \tag{18}$$

$$\hat{E}_{yh} = 0, \text{ on } x = a, b, \tag{19}$$

$$\hat{H}_h = H_h^{(in)}, \text{ on } \partial\Omega. \tag{20}$$

3.1 The stability analysis

In this subsection, we will show that the solutions of our proposed semi-discrete DG method satisfy the same energy identity as in the continuous level (8), which leads to the stability of the method.

Theorem 3.1. *For the semi-discrete DG method* (11)-(14) *with alternating fluxes* (15)-(20)*, we define the energy:*

$$\begin{aligned} ENG_h(t) :=& \Bigg[||\partial_t \boldsymbol{D}_h||^2 + ||M_C^{\frac{1}{2}} \boldsymbol{D}_h||^2 + \epsilon_0 \lambda_2 \left(||M_A^{-\frac{1}{2}} \partial_{t^2} \boldsymbol{E}_h||^2 + 2\omega_p^2 ||M_A^{-\frac{1}{2}} \partial_t \boldsymbol{E}_h||^2 + \omega_p^4 ||M_A^{-\frac{1}{2}} \boldsymbol{E}_h||^2 \right) \\ &+ \mu_0 \mu \left(\omega_p^2 ||\partial_t H_h||^2 + ||\partial_{t^2} H_h||^2 \right) \Bigg](t), \end{aligned} \tag{21}$$

then, the energy satisfies the following energy identity: For any $t \geq 0$*:*

$$\begin{aligned} &ENG_h(t) = ENG_h(0) \\ &+ 2 \int_0^t \left[\epsilon_0 \lambda_2 \left(M_A^{-1} \partial_{t^2} \boldsymbol{E}_h + \omega_p^2 M_A^{-1} \boldsymbol{E}_h, \partial_t \boldsymbol{D}_h \right) + \left(M_C \partial_t \boldsymbol{D}_h, \partial_{t^2} \boldsymbol{E}_h \right) + \omega_p^2 \left(M_C \boldsymbol{D}_h, \partial_t \boldsymbol{E}_h \right) \right](s) ds. \end{aligned} \tag{22}$$

Furthermore, it leads to the stability:

$$ENG_h(t) \leq \exp(C^* t) \cdot ENG_h(0), \qquad \forall t \in [0, T], \tag{23}$$

with the constant C^* *depending only on the physical parameters* $\varepsilon_0, \mu_0, d, H_1, H_2$ *and* ω_p*.*

Proof. To make our proof easy to follow, we divide the proof into several major parts.

(I) Choosing $\boldsymbol{u} = \partial_t \boldsymbol{D}_h$ in (13), we obtain

$$\frac{1}{2} \frac{d}{dt} \left[||\partial_t \boldsymbol{D}_h||^2 + ||M_C^{\frac{1}{2}} \boldsymbol{D}_h||^2 \right] = \epsilon_0 \lambda_2 \left(M_A^{-1} \partial_{t^2} \boldsymbol{E}_h + \omega_p^2 M_A^{-1} \boldsymbol{E}_h, \partial_t \boldsymbol{D}_h \right). \tag{24}$$

Differentiating (13) with respect to t and choosing $\boldsymbol{u} = \partial_{t^2} \boldsymbol{E}_h$, we have

$$\frac{\epsilon_0 \lambda_2}{2} \frac{d}{dt} \left[||M_A^{-\frac{1}{2}} \partial_{t^2} \boldsymbol{E}_h||^2 + \omega_p^2 ||M_A^{-\frac{1}{2}} \partial_t \boldsymbol{E}_h||^2 \right] = \left(\partial_{t^3} \boldsymbol{D}_h + M_C \partial_t \boldsymbol{D}_h, \partial_{t^2} \boldsymbol{E}_h \right). \tag{25}$$

Adding (24) and (25) together, we obtain

$$\begin{aligned} &\frac{1}{2} \frac{d}{dt} \left[||\partial_t \boldsymbol{D}_h||^2 + ||M_C^{\frac{1}{2}} \boldsymbol{D}_h||^2 + \epsilon_0 \lambda_2 \left(||M_A^{-\frac{1}{2}} \partial_{t^2} \boldsymbol{E}_h||^2 + \omega_p^2 ||M_A^{-\frac{1}{2}} \partial_t \boldsymbol{E}_h||^2 \right) \right] \\ &= \epsilon_0 \lambda_2 \left(M_A^{-1} \partial_{t^2} \boldsymbol{E}_h + \omega_p^2 M_A^{-1} \boldsymbol{E}_h, \partial_t \boldsymbol{D}_h \right) + \left(\partial_{t^3} \boldsymbol{D}_h + M_C \partial_t \boldsymbol{D}_h, \partial_{t^2} \boldsymbol{E}_h \right). \end{aligned} \tag{26}$$

(II) To control the term $\boldsymbol{E}_h$ on the right hand side (RHS) of (26), we choose $\boldsymbol{u} = \partial_t \boldsymbol{E}_h$ in (13) to obtain

$$\frac{\epsilon_0 \lambda_2}{2} \frac{d}{dt} \left[||M_A^{-\frac{1}{2}} \partial_t \boldsymbol{E}_h||^2 + \omega_p^2 ||M_A^{-\frac{1}{2}} \boldsymbol{E}_h||^2 \right] = \left(\partial_{t^2} \boldsymbol{D}_h + M_C \boldsymbol{D}_h, \partial_t \boldsymbol{E}_h \right). \tag{27}$$

Multiplying (27) by ω_p^2, then adding the result to (26), we have

$$\begin{aligned} &\frac{1}{2} \frac{d}{dt} \left[||\partial_t \boldsymbol{D}_h||^2 + ||M_C^{\frac{1}{2}} \boldsymbol{D}_h||^2 + \epsilon_0 \lambda_2 \left(||M_A^{-\frac{1}{2}} \partial_{t^2} \boldsymbol{E}_h||^2 + 2\omega_p^2 ||M_A^{-\frac{1}{2}} \partial_t \boldsymbol{E}_h||^2 + \omega_p^4 ||M_A^{-\frac{1}{2}} \boldsymbol{E}_h||^2 \right) \right] \\ &= \epsilon_0 \lambda_2 \left(M_A^{-1} \partial_{t^2} \boldsymbol{E}_h + \omega_p^2 M_A^{-1} \boldsymbol{E}_h, \partial_t \boldsymbol{D}_h \right) + \left(\partial_{t^3} \boldsymbol{D}_h + M_C \partial_t \boldsymbol{D}_h, \partial_{t^2} \boldsymbol{E}_h \right) + \omega_p^2 \left(\partial_{t^2} \boldsymbol{D}_h + M_C \boldsymbol{D}_h, \partial_t \boldsymbol{E}_h \right). \end{aligned} \tag{28}$$

(III) Now we need to control the terms $\partial_{t^3}\boldsymbol{D}_h$ and $\partial_{t^2}\boldsymbol{D}_h$ on the RHS of (28).

Differentiating both (11) and (12) with respect to t, choosing $\phi_x = \partial_t E_{xh}$ and $\phi_y = \partial_t E_{yh}$ in (11) and (12), respectively, then adding the results together, we have

$$\begin{aligned}&\int_e \partial_{t^2}\boldsymbol{D}_h \cdot \partial_t \boldsymbol{E}_h + \int_e \partial_t H_h(\partial_y \partial_t E_{xh} - \partial_x \partial_t E_{yh}) \\ &- \int_{\partial e} \partial_t \hat{H}_h \partial_t E_{xh}^{(\mathrm{in})} n_y^{(in)} + \int_{\partial e} \partial_t \hat{H}_h \partial_t E_{yh}^{(\mathrm{in})} n_x^{(in)} = 0.\end{aligned} \tag{29}$$

Differentiating (14) with respect to t, choosing $\psi = \partial_t H_h$, then using integration by parts, we have

$$\begin{aligned}&\mu_0\mu \int_e \partial_{t^2} H_h \partial_t H_h + \int_e \partial_t H_h(\partial_x \partial_t E_{yh} - \partial_y \partial_t E_{xh}) - \int_{\partial e} \partial_t E_{yh}^{(\mathrm{in})} \partial_t H_h^{(in)} n_x^{(in)} \\ &+ \int_{\partial e} \partial_t E_{xh}^{(\mathrm{in})} \partial_t H_h^{(in)} n_y^{(in)} + \int_{\partial e} (\partial_t \hat{E}_{yh} n_x^{(\mathrm{in})} - \partial_t \hat{E}_{xh} n_y^{(in)}) \partial_t H_h^{(in)} = 0.\end{aligned} \tag{30}$$

Adding (29) and (30) together over all elements, we have

$$\sum_{e\in\mathcal{T}_h} \int_e \partial_{t^2}\boldsymbol{D}_h \cdot \partial_t \boldsymbol{E}_h + \frac{\mu_0\mu}{2}\frac{d}{dt}||\partial_t H_h||^2 + F_x - F_y = 0, \tag{31}$$

where we denote

$$F_x = \sum_{e\in\mathcal{T}_h} \int_{\partial e} \left(-\partial_t \hat{H}_h \partial_t E_{xh}^{(in)} n_y^{(in)} + \partial_t H_h^{(in)} \partial_t E_{xh}^{(in)} n_y^{(in)} - \partial_t H_h^{(in)} \partial_t \hat{E}_{xh} n_y^{(in)}\right), \tag{32}$$

$$F_y = \sum_{e\in\mathcal{T}_h} \int_{\partial e} \left(\partial_t \hat{H}_h \partial_t E_{yh}^{(in)} n_x^{(in)} - \partial_t H_h^{(in)} \partial_t E_{yh}^{(in)} n_x^{(in)} + \partial_t H_h^{(in)} \partial_t \hat{E}_{yh} n_x^{(in)}\right). \tag{33}$$

By regrouping terms by sides of the elements and using the definitions of the numerical fluxes $\hat{H}_h$ and $\hat{E}_{xh}$, we have:

$$\begin{aligned}F_x = &\sum_{s\in\mathcal{S}_I} n_y^R \int_s \left(-\partial_t H_h^L \partial_t E_{xh}^R + \partial_t H_h^L \partial_t E_{xh}^L + \partial_t H_h^R \partial_t E_{xh}^R - \partial_t H_h^L \partial_t E_{xh}^L - \partial_t H_h^R \partial_t E_{xh}^R + \partial_t H_h^L \partial_t E_{xh}^R\right) \\ &+ \sum_{s\in\mathcal{S}_{Top}} n_y^R \int_s \left(-\partial_t \hat{H}_h \partial_t E_{xh}^{(in)} + \partial_t H_h^{(in)} \partial_t E_{xh}^{(in)} - \partial_t H_h^{(in)} \partial_t \hat{E}_{xh}\right) \\ &+ \sum_{s\in\mathcal{S}_{Bottom}} n_y^R \int_s \left(-\partial_t \hat{H}_h \partial_t E_{xh}^{(in)} + \partial_t H_h^{(in)} \partial_t E_{xh}^{(in)} - \partial_t H_h^{(in)} \partial_t \hat{E}_{xh}\right) = 0,\end{aligned} \tag{34}$$

where $\mathcal{S}_I$ denotes the set of all non-boundary sides, $\mathcal{S}_{Top}$ represents the set of sides on $y = d$, and $\mathcal{S}_{Bottom}$ on $y = c$.

Similarly, we can prove that $F_y = 0$.

Then using the results of $F_x = F_y = 0$ in (31), we obtain

$$\sum_{e\in\mathcal{T}_h}\int_e \partial_{t^2}\boldsymbol{D}_h\cdot\partial_t\boldsymbol{E}_h = -\frac{\mu_0\mu}{2}\frac{d}{dt}||\partial_t H_h||^2. \tag{35}$$

Following the same argument, we can prove that

$$\sum_{e\in\mathcal{T}_h}\int_e \partial_{t^3}\boldsymbol{D}_h\cdot\partial_{t^2}\boldsymbol{E}_h = -\frac{\mu_0\mu}{2}\frac{d}{dt}||\partial_{t^2} H_h||^2. \tag{36}$$

Substituting (35) and (36) into (28), we obtain

$$\begin{aligned}&\frac{1}{2}\frac{d}{dt}\Big[||\partial_t\boldsymbol{D}_h||^2 + ||M_C^{\frac{1}{2}}\boldsymbol{D}_h||^2 + \epsilon_0\lambda_2\left(||M_A^{-\frac{1}{2}}\partial_{t^2}\boldsymbol{E}_h||^2 + 2\omega_p^2||M_A^{-\frac{1}{2}}\partial_t\boldsymbol{E}_h||^2 + \omega_p^4||M_A^{-\frac{1}{2}}\boldsymbol{E}_h||^2\right)\\ &\quad + \mu_0\mu\left(\omega_p^2||\partial_t H_h||^2 + ||\partial_{t^2}H_h||^2\right)\Big]\\ &= \epsilon_0\lambda_2\left(M_A^{-1}\partial_{t^2}\boldsymbol{E}_h + \omega_p^2 M_A^{-1}\boldsymbol{E}_h, \partial_t\boldsymbol{D}_h\right) + \left(M_C\partial_t\boldsymbol{D}_h, \partial_{t^2}\boldsymbol{E}_h\right) + \omega_p^2\left(M_C\boldsymbol{D}_h, \partial_t\boldsymbol{E}_h\right).\end{aligned} \tag{37}$$

Integrating (37) with respect to t from 0 to t, we obtain the energy identity (22). Then we apply the Cauchy-Schwarz inequality to all terms in the RHS of (37), and use the Gronwall inequality to complete the proof.

□

3.2 The error analysis

In this section, we will show the sub-optimal error estimate of the semi-discrete DG method on unstructured meshes, and the optimal error estimate of the DG method with a modified alternating flux on tensor-product rectangular meshes with tensor-product DG spaces.

3.2.1 The error analysis on unstructured meshes

Denote the errors between the exact solutions (E_x, E_y, D_x, D_y, H) of (1)-(4) and the corresponding numerical solutions $(E_{xh}, E_{yh}, D_{xh}, D_{yh}, H_h)$ of the semi-discrete scheme (11)-(14) as

$$\mathcal{E}_{E_x} = E_x - E_{xh},\ \mathcal{E}_{E_y} = E_y - E_{yh},\ \mathcal{E}_{D_x} = D_x - D_{xh},\ \mathcal{E}_{D_y} = D_y - D_{yh},\ \mathcal{E}_H = H - H_h,$$

and define $\mathcal{E}_{\boldsymbol{D}} = (\mathcal{E}_{D_x},\ \mathcal{E}_{D_y})$, and $\mathcal{E}_{\boldsymbol{E}} = (\mathcal{E}_{E_x},\ \mathcal{E}_{E_y})$.

Subtracting (11)-(14) from the weak formulation of the PDEs (1)-(4), we obtain the following error equations:

$$\int_e \partial_t\mathcal{E}_{D_x}\phi_x + \int_e \mathcal{E}_H\partial_y\phi_x - \int_{\partial e}\hat{\mathcal{E}}_H\phi_x^{(\mathrm{in})}n_y^{(in)} = 0, \tag{38}$$

$$\int_e \partial_t\mathcal{E}_{D_y}\phi_y - \int_e \mathcal{E}_H\partial_x\phi_y + \int_{\partial e}\hat{\mathcal{E}}_H\phi_y^{(\mathrm{in})}n_x^{(in)} = 0, \tag{39}$$

$$\varepsilon_0\lambda_2\int_e\left(M_A^{-1}\partial_{t^2}\mathcal{E}_{\boldsymbol{E}} + \omega_p^2 M_A^{-1}\mathcal{E}_{\boldsymbol{E}}\right)\cdot\boldsymbol{u} = \int_e\left(\partial_{t^2}\mathcal{E}_{\boldsymbol{D}} + M_C\mathcal{E}_{\boldsymbol{D}}\right)\cdot\boldsymbol{u}, \tag{40}$$

$$\mu_0\mu\int_e\partial_t\mathcal{E}_H\psi - \int_e\mathcal{E}_{E_y}\partial_x\psi + \int_e\mathcal{E}_{E_x}\partial_y\psi + \int_{\partial e}(\hat{\mathcal{E}}_{E_y}n_x^{(in)} - \hat{\mathcal{E}}_{E_x}n_y^{(in)})\psi^{(\mathrm{in})} = 0. \tag{41}$$

Then, we have the following theorem:

Theorem 3.2. *Suppose that the analytical solutions (E_x, E_y, D_x, D_y, H) of (1)-(4) are smooth enough, and $(E_{xh}, E_{yh}, D_{xh}, D_{yh}, H_h)$ are the corresponding numerical solutions of (11)-(14). With the alternating flux (15)-(17) and the PEC boundary condition (18)-(20), we have the following error estimate:*

$$\begin{aligned}
&\Bigg[||\partial_t \boldsymbol{D} - \partial_t \boldsymbol{D}_h||^2 + ||M_C^{\frac{1}{2}}(\boldsymbol{D} - \boldsymbol{D}_h)||^2 + \epsilon_0\lambda_2 \Bigg(||M_A^{-\frac{1}{2}}\partial_{t^2}(\boldsymbol{E} - \partial_{t^2}\boldsymbol{E}_h)||^2 + 2\omega_p^2||M_A^{-\frac{1}{2}}(\partial_t \boldsymbol{E} - \partial_t \boldsymbol{E}_h)||^2 \\
&\qquad + \omega_p^4||M_A^{-\frac{1}{2}}(\boldsymbol{E} - \boldsymbol{E}_h)||^2 \Bigg) + \mu_0\mu\left(\omega_p^2||\partial_t H - \partial_t H_h||^2 + ||\partial_{t^2} H - \partial_{t^2} H_h||^2\right) \Bigg](t) \\
&\leq Ch^{2k} + \Bigg[||\partial_t \boldsymbol{D} - \partial_t \boldsymbol{D}_h||^2 + ||M_C^{\frac{1}{2}}(\boldsymbol{D} - \boldsymbol{D}_h)||^2 + \epsilon_0\lambda_2 \Bigg(||M_A^{-\frac{1}{2}}\partial_{t^2}(\boldsymbol{E} - \partial_{t^2}\boldsymbol{E}_h)||^2 \\
&+ 2\omega_p^2||M_A^{-\frac{1}{2}}(\partial_t \boldsymbol{E} - \partial_t \boldsymbol{E}_h)||^2 + \omega_p^4||M_A^{-\frac{1}{2}}(\boldsymbol{E} - \boldsymbol{E}_h)||^2 \Bigg) + \mu_0\mu\left(\omega_p^2||\partial_t H - \partial_t H_h||^2 + ||\partial_{t^2} H - \partial_{t^2} H_h||^2\right) \Bigg](0).
\end{aligned} \tag{42}$$

Here $k \geq 1$ is the order of the basis function V_h^k, and C is a positive constant independent of the mesh size h.

Proof. We first decompose each of the error function $(\mathcal{E}_{E_x}, \mathcal{E}_{E_y}, \mathcal{E}_{D_x}, \mathcal{E}_{D_y}, \mathcal{E}_H)$ into two parts respectively:

$$\begin{aligned}
\mathcal{E}_{E_x} = E_x - E_{xh} &= (\Pi E_x - E_{xh}) - (\Pi E_x - E_x) := \ \xi_{E_x} - \eta_{E_x}, \\
\mathcal{E}_{E_y} = E_y - E_{yh} &= (\Pi E_y - E_{yh}) - (\Pi E_y - E_y) := \ \xi_{E_y} - \eta_{E_y}, \\
\mathcal{E}_{D_x} = D_x - D_{xh} &= (\Pi D_x - D_{xh}) - (\Pi D_x - D_x) := \ \xi_{D_x} - \eta_{D_x}, \\
\mathcal{E}_{D_y} = D_y - D_{yh} &= (\Pi D_y - D_{yh}) - (\Pi D_y - D_y) := \ \xi_{D_y} - \eta_{D_y}, \\
\mathcal{E}_H \ = \ H - H_h \ &= \ (\Pi H - H_h) - (\Pi H - H) \ := \ \xi_H - \eta_H,
\end{aligned}$$

where Π presents the standard L_2 projection onto V_h^k.

Similar as the stability proof, we take $\boldsymbol{u} = \partial_t \xi_{\boldsymbol{D}} =$ and $\boldsymbol{u} = \partial_t \xi_{\boldsymbol{E}}$ respectively in (40), and we differentiate (40) with respect to t and let $\boldsymbol{u} = \partial_{t^2}\xi_{\boldsymbol{D}}$. Then we sum over all elements in the domain. By putting all terms containing η to the RHS, and the rest terms to the left hand side (LHS), we get:

$$\begin{aligned}
&\frac{1}{2}\frac{d}{dt}\left[||\partial_t \xi_{\boldsymbol{D}}||^2 + ||M_C^{\frac{1}{2}}\xi_{\boldsymbol{D}}||^2\right] - \epsilon_0\lambda_2\left(M_A^{-1}\partial_{t^2}\xi_{\boldsymbol{E}} + \omega_p^2 M_A^{-1}\xi_{\boldsymbol{E}}, \partial_t \xi_{\boldsymbol{D}}\right) = \\
&\left(\partial_{t^2}\eta_{\boldsymbol{D}}, \partial_t \xi_{\boldsymbol{D}}\right) + \left(M_C \eta_{\boldsymbol{D}}, \partial_t \xi_{\boldsymbol{D}}\right) - \varepsilon_0\lambda_2\left(M_A^{-1}\partial_{t^2}\eta_{\boldsymbol{E}} + M_A^{-1}\eta_{\boldsymbol{E}}, \partial_t \xi_{\boldsymbol{D}}\right),
\end{aligned} \tag{43}$$

$$\begin{aligned}
&\frac{\epsilon_0\lambda_2}{2}\frac{d}{dt}\left[||M_A^{-\frac{1}{2}}\partial_t \xi_{\boldsymbol{E}}||^2 + \omega_p^2||M_A^{-\frac{1}{2}}\xi_{\boldsymbol{E}}||^2\right] - \left(\partial_{t^2}\xi_{\boldsymbol{D}} + M_C\xi_{\boldsymbol{D}}, \partial_t \xi_{\boldsymbol{E}}\right) = \\
&\varepsilon_0\lambda_2\left(M_A^{-1}\partial_{t^2}\eta_{\boldsymbol{E}}, \partial_t \xi_{\boldsymbol{E}}\right) + \varepsilon_0\lambda_2\omega_p^2\left(M_A^{-1}\eta_{\boldsymbol{E}}, \partial_t \xi_{\boldsymbol{E}}\right) - \left(\partial_{t^2}\eta_{\boldsymbol{D}} + M_C\eta_{\boldsymbol{D}}, \partial_t \xi_{\boldsymbol{E}}\right),
\end{aligned} \tag{44}$$

$$\frac{\epsilon_0\lambda_2}{2}\frac{d}{dt}\left[||M_A^{-\frac{1}{2}}\partial_{t^2}\xi_{\boldsymbol{E}}||^2+\omega_p^2||M_A^{-\frac{1}{2}}\partial_t\xi_{\boldsymbol{E}}||^2\right]-\left(\partial_{t^3}\xi_{\boldsymbol{D}}+M_C\partial_t\xi_{\boldsymbol{D}},\partial_{t^2}\xi_{\boldsymbol{E}}\right)= \\ \varepsilon_0\lambda_2\left(M_A^{-1}\partial_{t^3}\eta_{\boldsymbol{E}},\partial_{t^2}\xi_{\boldsymbol{E}}\right)+\varepsilon_0\lambda_2\omega_p^2\left(M_A^{-1}\partial_t\eta_{\boldsymbol{E}},\partial_{t^2}\xi_{\boldsymbol{E}}\right)-\left(\partial_{t^3}\eta_{\boldsymbol{D}}+M_C\partial_t\eta_{\boldsymbol{D}},\partial_{t^2}\xi_{\boldsymbol{E}}\right), \tag{45}$$

where $\xi_{\boldsymbol{D}}=(\xi_{D_x},\xi_{D_y})$, and $\xi_{\boldsymbol{E}}=(\xi_{E_x},\xi_{E_y})$. $\eta_{\boldsymbol{D}}$ and $\eta_{\boldsymbol{E}}$ are defined similarly.

Next, we differentiate (38), (39), and (41) with respect to t, and choose $\phi_x=\partial_t\xi_{E_x}$, $\phi_y=\partial_t\xi_{E_y}$ and $\psi=\partial_t\xi_H$ respectively. Then we sum up these three equations, and sum over all elements in the domain to obtain:

$$\left(\partial_{t^2}\mathcal{E}_{\boldsymbol{D}},\partial_t\xi_{\boldsymbol{E}}\right)+\mu_0\mu(\partial_{t^2}\mathcal{E}_H,\partial_t\xi_H)+\left(\partial_t\mathcal{E}_H,\partial_y\partial_t\xi_{E_x}-\partial_x\partial_t\xi_{E_y}\right)-(\partial_t\mathcal{E}_{E_y},\partial_x\partial_t\xi_H)+(\partial_t\mathcal{E}_{E_x},\partial_y\partial_t\xi_H) \\ \sum_{e\in\mathcal{T}_h}\left(-\int_{\partial e}\partial_t\hat{\mathcal{E}}_H\partial_t\xi_{E_x}^{(\mathrm{in})}n_y^{(in)}+\int_{\partial e}\partial_t\hat{\mathcal{E}}_H\partial_t\xi_{E_y}^{(\mathrm{in})}n_x^{(in)}+\int_{\partial e}(\partial_t\hat{\mathcal{E}}_{E_y}n_x^{(\mathrm{in})}-\partial_t\hat{\mathcal{E}}_{E_x}n_y^{(in)})\partial_t\xi_H^{(in)}\right)=0. \tag{46}$$

By applying the error decomposition, we have:

$$\left(\partial_{t^2}\xi_{\boldsymbol{D}},\partial_t\xi_{\boldsymbol{E}}\right)+\mu_0\mu(\partial_{t^2}\xi_H,\partial_t\xi_H)+\left(\partial_t\xi_H,\partial_y\partial_t\xi_{E_x}-\partial_x\partial_t\xi_{E_y}\right)-(\partial_t\xi_{E_y},\partial_x\partial_t\xi_H)+(\partial_t\xi_{E_x},\partial_y\partial_t\xi_H) \\ \sum_{e\in\mathcal{T}_h}\left(-\int_{\partial e}\partial_t\hat{\xi}_H\partial_t\xi_{E_x}^{(\mathrm{in})}n_y^{(in)}+\int_{\partial e}\partial_t\hat{\xi}_H\partial_t\xi_{E_y}^{(\mathrm{in})}n_x^{(in)}+\int_{\partial e}(\partial_t\hat{\xi}_{E_y}n_x^{(\mathrm{in})}-\partial_t\hat{\xi}_{E_x}n_y^{(in)})\partial_t\xi_H^{(in)}\right) \\ =\left(\partial_{t^2}\eta_{\boldsymbol{D}},\partial_t\xi_{\boldsymbol{E}}\right)+\mu_0\mu(\partial_{t^2}\eta_H,\partial_t\xi_H)+\left(\partial_t\eta_H,\partial_y\partial_t\xi_{E_x}-\partial_x\partial_t\xi_{E_y}\right)-(\partial_t\eta_{E_y},\partial_x\partial_t\xi_H)+(\partial_t\eta_{E_x},\partial_y\partial_t\xi_H) \\ \sum_{e\in\mathcal{T}_h}\left(-\int_{\partial e}\partial_t\hat{\eta}_H\partial_t\xi_{E_x}^{(\mathrm{in})}n_y^{(in)}+\int_{\partial e}\partial_t\hat{\eta}_H\partial_t\xi_{E_y}^{(\mathrm{in})}n_x^{(in)}+\int_{\partial e}(\partial_t\hat{\eta}_{E_y}n_x^{(\mathrm{in})}-\partial_t\hat{\eta}_{E_x}n_y^{(in)})\partial_t\xi_H^{(in)}\right). \tag{47}$$

Using the same argument as the stability analysis on the LHS, we obtain:

$$\left(\partial_{t^2}\xi_{\boldsymbol{D}},\partial_t\xi_{\boldsymbol{E}}\right)+\frac{\mu_0\mu}{2}\partial_t\|\partial_t\xi_H\|^2= \\ \left(\partial_{t^2}\eta_{\boldsymbol{D}},\partial_t\xi_{\boldsymbol{E}}\right)+\mu_0\mu(\partial_{t^2}\eta_H,\partial_t\xi_H)+\left(\partial_t\eta_H,\partial_y\partial_t\xi_{E_x}-\partial_x\partial_t\xi_{E_y}\right)-(\partial_t\eta_{E_y},\partial_x\partial_t\xi_H)+(\partial_t\eta_{E_x},\partial_y\partial_t\xi_H) \\ \sum_{e\in\mathcal{T}_h}\left(-\int_{\partial e}\partial_t\hat{\eta}_H\partial_t\xi_{E_x}^{(\mathrm{in})}n_y^{(in)}+\int_{\partial e}\partial_t\hat{\eta}_H\partial_t\xi_{E_y}^{(\mathrm{in})}n_x^{(in)}+\int_{\partial e}(\partial_t\hat{\eta}_{E_y}n_x^{(\mathrm{in})}-\partial_t\hat{\eta}_{E_x}n_y^{(in)})\partial_t\xi_H^{(in)}\right). \tag{48}$$

Similarly, by differentiating (38), (39), and (41) with respect to t^2, and choosing $\phi_x=\partial_{t^2}\xi_{E_x}$, $\phi_y=\partial_{t^2}\xi_{E_y}$ and $\psi=\partial_{t^2}\xi_H$ respectively, we have:

$$\left(\partial_{t^3}\xi_{\boldsymbol{D}},\partial_{t^2}\xi_{\boldsymbol{E}}\right)+\frac{\mu_0\mu}{2}\partial_t\|\partial_{t^2}\xi_H\|^2= \\ \left(\partial_{t^3}\eta_{\boldsymbol{D}},\partial_{t^2}\xi_{\boldsymbol{E}}\right)+\mu_0\mu(\partial_{t^3}\eta_H,\partial_{t^2}\xi_H)+\left(\partial_{t^2}\eta_H,\partial_y\partial_{t^2}\xi_{E_x}-\partial_x\partial_{t^2}\xi_{E_y}\right)-(\partial_{t^2}\eta_{E_y},\partial_x\partial_{t^2}\xi_H)+(\partial_{t^2}\eta_{E_x},\partial_y\partial_{t^2}\xi_H) \\ \sum_{e\in\mathcal{T}_h}\left(-\int_{\partial e}\partial_{t^2}\hat{\eta}_H\partial_{t^2}\xi_{E_x}^{(\mathrm{in})}n_y^{(in)}+\int_{\partial e}\partial_{t^2}\hat{\eta}_H\partial_{t^2}\xi_{E_y}^{(\mathrm{in})}n_x^{(in)}+\int_{\partial e}(\partial_{t^2}\hat{\eta}_{E_y}n_x^{(\mathrm{in})}-\partial_{t^2}\hat{\eta}_{E_x}n_y^{(in)})\partial_{t^2}\xi_H^{(in)}\right). \tag{49}$$

We multiply (44) and (48) by ω_p^2 and sum them with (43), (45) and (49) to attain the formula with the LHS equaling to:

$$\begin{aligned} LHS = \frac{1}{2}\frac{d}{dt}\Bigg[& ||\partial_t \xi_{\boldsymbol{D}}||^2 + ||M_C^{\frac{1}{2}} \xi_{\boldsymbol{D}}||^2 + \epsilon_0 \lambda_2 \left(||M_A^{-\frac{1}{2}} \partial_{t^2} \xi_{\boldsymbol{E}}||^2 + 2\omega_p^2 ||M_A^{-\frac{1}{2}} \partial_t \xi_{\boldsymbol{E}}||^2 + \omega_p^4 ||M_A^{-\frac{1}{2}} \xi_{\boldsymbol{E}}||^2 \right) \\ & + \mu_0 \mu \left(\omega_p^2 ||\partial_t \xi_H||^2 + ||\partial_{t^2} \xi_H||^2 \right) \Bigg] - \epsilon_0 \lambda_2 \left(M_A^{-1} \partial_{t^2} \xi_{\boldsymbol{E}} + \omega_p^2 M_A^{-1} \xi_{\boldsymbol{E}}, \partial_t \xi_{\boldsymbol{D}} \right) \\ & - \left(M_C \partial_t \xi_{\boldsymbol{D}}, \partial_{t^2} \xi_{\boldsymbol{E}} \right) - \omega_p^2 \left(M_C \xi_{\boldsymbol{D}}, \partial_t \xi_{\boldsymbol{E}} \right). \end{aligned} \tag{50}$$

Next, we consider the RHS. Using the fact that ξ_{E_x}, ξ_{E_y}, ξ_{D_x}, ξ_{D_y} and ξ_H are in space $P_k(e)$, the property of the projections $(\Pi u)_t = \Pi u_t$, and the definition of the L_2 projections:

$$\int_e (\Pi u - u) v dx = 0 \quad \forall v \in \mathcal{P}_k(e),$$

we conclude that all inner products of η and ξ terms equal to zero. Therefore, we obtain:

$$\begin{aligned} RHS = \sum_{e \in \mathcal{T}_h} \Bigg(& \omega_p^2 \left(- \int_{\partial e} \partial_t \hat{\eta}_H \partial_t \xi_{E_x}^{(\text{in})} n_y^{(in)} + \int_{\partial e} \partial_t \hat{\eta}_H \partial_t \xi_{E_y}^{(\text{in})} n_x^{(in)} + \int_{\partial e} (\partial_t \hat{\eta}_{E_y} n_x^{(\text{in})} - \partial_t \hat{\eta}_{E_x} n_y^{(in)}) \partial_t \xi_H^{(in)} \right) \\ & - \int_{\partial e} \partial_{t^2} \hat{\eta}_H \partial_{t^2} \xi_{E_x}^{(\text{in})} n_y^{(in)} + \int_{\partial e} \partial_{t^2} \hat{\eta}_H \partial_{t^2} \xi_{E_y}^{(\text{in})} n_x^{(in)} + \int_{\partial e} (\partial_{t^2} \hat{\eta}_{E_y} n_x^{(\text{in})} - \partial_{t^2} \hat{\eta}_{E_x} n_y^{(in)}) \partial_{t^2} \xi_H^{(in)} \Bigg). \end{aligned} \tag{51}$$

Consider the first term on the RHS, by applying the Cauchy-Schwarz inequality firstly, and using the approximating property of polynomial preserving operators (Theorem 3.4.1 in [9]) on the η_H and the standard inverse inequality [9] on the ξ_{E_x}, we have

$$\begin{aligned} \sum_{e \in \mathcal{T}_h} \int_{\partial e} \partial_t \hat{\eta}_H \partial_t \xi_{E_x}^{(\text{in})} n_y^{(in)} & \leq \sum_{e \in \mathcal{T}} \frac{1}{\delta h} \int_{\partial e} \left| \partial_t \hat{\eta}_H \right|^2 + \delta h \int_{\partial e} \left| \partial_t \xi_{E_x}^{(\text{in})} \right|^2 \\ & \leq C \sum_{e \in \mathcal{T}_h} \left(\frac{1}{\delta} ||\partial_t \eta_H||_{L^\infty(e)}^2 + \delta h^2 ||\partial_t \xi_{E_x}||_{L^\infty(e)}^2 \right) \\ & \leq C h^{2k} ||\partial_t H||_{H^{k+1}(\Omega)}^2 + C ||\partial_t \xi_{E_x}||_{L^2(\Omega)}^2, \end{aligned} \tag{52}$$

with any $\delta > 0$. Note that the constant Cs may have different values in each term, but they are all independent of the mesh size h.

Using the same arguments on the remaining terms, we obtain the following inequality:

$$\frac{1}{2}\frac{d}{dt}\Bigg[||\partial_t\xi_{\boldsymbol{D}}||^2+||M_C^{\frac{1}{2}}\xi_{\boldsymbol{D}}||^2+\epsilon_0\lambda_2\left(||M_A^{-\frac{1}{2}}\partial_{t^2}\xi_{\boldsymbol{E}}||^2+2\omega_p^2||M_A^{-\frac{1}{2}}\partial_t\xi_{\boldsymbol{E}}||^2+\omega_p^4||M_A^{-\frac{1}{2}}\xi_{\boldsymbol{E}}||^2\right)$$
$$+\mu_0\mu\left(\omega_p^2||\partial_t\xi_H||^2+||\partial_{t^2}\xi_H||^2\right)\Bigg]\leq Ch^{2k}\left(||\partial_t\boldsymbol{E}||^2_{H^{k+1}}+||\partial_{t^2}\boldsymbol{E}||^2_{H^{k+1}}+||\partial_t H||^2_{H^{k+1}}+||\partial_{t^2}H||^2_{H^{k+1}}\right)$$
$$+C\left(||\partial_t\xi_{\boldsymbol{E}}||^2+||\partial_{t^2}\xi_{\boldsymbol{E}}||^2+||\partial_t\xi_H||^2+||\partial_{t^2}\xi_H||^2\right)+\epsilon_0\lambda_2\left(M_A^{-1}\partial_{t^2}\xi_{\boldsymbol{E}}+\omega_p^2M_A^{-1}\xi_{\boldsymbol{E}},\partial_t\xi_{\boldsymbol{D}}\right)$$
$$+\left(M_C\partial_t\xi_{\boldsymbol{D}},\partial_{t^2}\xi_{\boldsymbol{E}}\right)+\omega_p^2\left(M_C\xi_{\boldsymbol{D}},\partial_t\xi_{\boldsymbol{E}}\right). \tag{53}$$

Finally, applying the Cauchy-Schwarz inequality, and then using the Gronwall inequality, the error estimates of the L_2 projections, and the triangle inequality, we can conclude the proof. □

3.2.2 The error analysis on rectangular meshes

In general, using the flux and boundary condition (15)-(20), the stability and error analysis on tensor-product rectangular meshes are the same as those on triangular meshes. However, inspired by [33], if we modify the fluxes at the PEC boundary by adding suitable jump terms, and by using tensor-product DG spaces, the optimal error accuracy can be proved mathematically, and can be observed in the numerical tests.

We firstly define the rectangular mesh. For simplicity, we consider a rectangular domain $\Omega=[a_x,b_x]\times[a_y,b_y]$, which is discretized by the cells $I_{ij}=[x_{i-\frac{1}{2}},x_{i+\frac{1}{2}}]\times[y_{j-\frac{1}{2}},y_{j+\frac{1}{2}}]$ for $1\leq i\leq N_x$ and $1\leq j\leq N_y$. The mesh sizes are defined as $h_i^x=x_{i+\frac{1}{2}}-x_{i-\frac{1}{2}}$ and $h_j^y=y_{j+\frac{1}{2}}-y_{j-\frac{1}{2}}$, with $h^x=\max_{1\leq i\leq N_x}h_i^x$, $h^y=\max_{1\leq j\leq N_y}h_j^y$, and $h=\max(h^x,h^y)$. The finite element space V_h^k is chosen as

$$V_h^k=\{v:v|_{I_{ij}}\in Q^k(I_{ij})\},$$

where $Q^k(I_{ij})$ is the space of the tensor products of one dimensional polynomials with degree at most k over the cell I_{ij}. For simplicity, we denote $u_h(x^+_{i+\frac{1}{2}},y)$ (or $u_h^+(x_{i+\frac{1}{2}},y)$ or $(u_h)^+_{i+\frac{1}{2},y}$) and $u_h(x^-_{i+\frac{1}{2}},y)$ (or $u_h^-(x_{i+\frac{1}{2}},y)$ or $(u_h)^-_{i+\frac{1}{2},y}$) as the limit value of u_h at $x_{i+\frac{1}{2}}$ from the right cell $I_{i+1,j}$, and from the left cell $I_{i,j}$ respectively. $u_h(x,y^+_{j+\frac{1}{2}})$ (or $u_h^+(x,y_{j+\frac{1}{2}})$ or $(u_h)^+_{x,j+\frac{1}{2}}$), and $u_h(x,y^-_{j+\frac{1}{2}})$ (or $u_h^-(x,y_{j+\frac{1}{2}})$ or $(u_h)^-_{x,j+\frac{1}{2}}$) are defined similarly. By setting the fixed direction $\boldsymbol{\beta}=(1,1)$, the alternating fluxes become:

$$\hat{E}_{xh}(x,y_{j+\frac{1}{2}})=E^+_{xh}(x,y_{j+\frac{1}{2}}), \tag{54}$$
$$\hat{E}_{yh}(x_{i+\frac{1}{2}},y)=E^+_{yh}(x_{i+\frac{1}{2}},y), \tag{55}$$
$$\hat{H}_h(x,y_{j+\frac{1}{2}})=H^-_h(x,y_{j+\frac{1}{2}}), \tag{56}$$
$$\hat{H}_h(x_{i+\frac{1}{2}},y)=H^-_h(x_{i+\frac{1}{2}},y). \tag{57}$$

To achieve the optimal convergence, instead of letting the fluxes $\hat{H}_h(x,y_{\frac{1}{2}})=H^+(x,y_{\frac{1}{2}})$ and

$\hat{H}_h(x_{\frac{1}{2}}, y) = H^+(x_{\frac{1}{2}}, y)$ as in (20), we apply the PEC boundary condition as stated below:

$$\hat{E}_{xh}(x, y_{\frac{1}{2}}) = 0, \tag{58}$$

$$\hat{E}_{yh}(x_{\frac{1}{2}}, y) = 0, \tag{59}$$

$$\hat{H}_h(x, y_{\frac{1}{2}}) = H_h^+(x, y_{\frac{1}{2}}) + c_0 \left[\!\!\left[E_{xh}(x, y_{\frac{1}{2}}) \right]\!\!\right], \tag{60}$$

$$\hat{H}_h(x_{\frac{1}{2}}, y) = H_h^+(x_{\frac{1}{2}}, y) - c_0 \left[\!\!\left[E_{yh}(x_{\frac{1}{2}}, y) \right]\!\!\right]. \tag{61}$$

The constant c_0 is independent of the mesh size h, and in the following numerical tests, c_0 is chosen as $\frac{1}{2}$. We denote $[\![u]\!] = u^+ - u^-$ as the jump cross the cell boundaries. Here $[\![E_{xh}(x, y_{\frac{1}{2}})]\!] = E_{xh}^+(x, y_{\frac{1}{2}}) - 0$, and $[\![E_{yh}(x_{\frac{1}{2}}, y)]\!] = E_{yh}^+(x_{\frac{1}{2}}, y) - 0$.

Using the fluxes and boundary conditions (54)-(61), and following the same argument as in section 3.1, we can verify the stability of the method. For the error analysis, we have the following theorem:

Theorem 3.3. *Suppose that the analytical solutions (E_x, E_y, D_x, D_y, H) of (1)-(4) are smooth enough, and $(E_{xh}, E_{yh}, D_{xh}, D_{yh}, H_h)$ are the corresponding numerical solutions of (11)-(14) on the rectangular mesh. With the alternating flux (54)-(57) and the PEC boundary condition (58)-(61), we have the following error estimate:*

$$\begin{aligned}
&\Bigg[||\partial_t \boldsymbol{D} - \partial_t \boldsymbol{D}_h||^2 + ||M_C^{\frac{1}{2}}(\boldsymbol{D} - \boldsymbol{D}_h)||^2 + \epsilon_0\lambda_2 \Big(||M_A^{-\frac{1}{2}} \partial_{t^2} \boldsymbol{E} - \partial_{t^2} \boldsymbol{E}_h||^2 + 2\omega_p^2 ||M_A^{-\frac{1}{2}}(\partial_t \boldsymbol{E} - \partial_t \boldsymbol{E}_h)||^2 \\
&\qquad + \omega_p^4 ||M_A^{-\frac{1}{2}}(\boldsymbol{E} - \boldsymbol{E}_h)||^2 \Big) + \mu_0\mu \left(\omega_p^2 ||\partial_t H - \partial_t H_h||^2 + ||\partial_{t^2} H - \partial_{t^2} H_h||^2 \right) \Bigg](t) \\
&\leq Ch^{2k+2} + \Bigg[||\partial_t \boldsymbol{D} - \partial_t \boldsymbol{D}_h||^2 + ||M_C^{\frac{1}{2}}(\boldsymbol{D} - \boldsymbol{D}_h)||^2 + \epsilon_0\lambda_2 \Big(||M_A^{-\frac{1}{2}} \partial_{t^2} \boldsymbol{E} - \partial_{t^2} \boldsymbol{E}_h||^2 \\
&+ 2\omega_p^2 ||M_A^{-\frac{1}{2}}(\partial_t \boldsymbol{E} - \partial_t \boldsymbol{E}_h)||^2 + \omega_p^4 ||M_A^{-\frac{1}{2}}(\boldsymbol{E} - \boldsymbol{E}_h)||^2 \Big) + \mu_0\mu \left(\omega_p^2 ||\partial_t H - \partial_t H_h||^2 + ||\partial_{t^2} H - \partial_{t^2} H_h||^2 \right) \Bigg](0).
\end{aligned} \tag{62}$$

The $k \geq 1$ is the order of the basis function V_h^k, and C is a positive constant independent of the mesh size h.

Proof. To prove the theorem, we firstly need to define some new projections [33]. The $1D$ projections in the x direction

$$P_x^{\pm} : H^1(I_i) \to \mathcal{P}_k(I_i)$$

are defined as the functions in the k-th degree polynomial space that satisfy

$$\int_{I_i} (P_x^+ u - u) v dx = 0 \quad \forall v \in \mathcal{P}_{k-1}(I_i), \qquad \text{and} \quad P_x^+ u(x_{i-\frac{1}{2}}^+) = u(x_{i-\frac{1}{2}}^+), \tag{63}$$

$$\int_{I_i}(P_x^- u - u)v dx = 0 \quad \forall v \in \mathcal{P}_{k-1}(I_i), \qquad \text{and} \quad P_x^- u(x^-_{i+\frac{1}{2}}) = u(x^-_{i+\frac{1}{2}}). \tag{64}$$

The $1D$ projections in the y direction $P_y^{\pm}$ are defined in the same way. Besides, we denote the standard L_2 projections in the x and y directions as

$$P_x : H^1(I_i) \to \mathcal{P}_k(I_i), \qquad P_y : H^1(I_i) \to \mathcal{P}_k(I_i).$$

Next, we use the tensor products of the $1D$ projections to define the $2D$ projections in cell I_{ij}. In particular, we define the projection

$$\Pi_1 = P_x \otimes P_y^+ : H^2(I_{ij}) \to Q_k(I_{ij}),$$

which satisfies that: For any $u \in H^2(I_{ij})$ and any test function $\phi \in Q_k(I_{ij})$:

$$\int_{I_{ij}} \Pi_1 u(x,y)\frac{\partial \phi(x,y)}{\partial y}dxdy = \int_{I_{ij}} u(x,y)\frac{\partial \phi(x,y)}{\partial y}dxdy, \tag{65}$$

$$\int_{I_i} \Pi_1 u\left(x, y^+_{j-\frac{1}{2}}\right)\phi\left(x, y^+_{j-\frac{1}{2}}\right)dx = \int_{I_i} u\left(x, y^+_{j-\frac{1}{2}}\right)\phi\left(x, y^+_{j-\frac{1}{2}}\right)dx. \tag{66}$$

The projection

$$\Pi_2 = P_x^+ \otimes P_y : H^2(I_{ij}) \to Q_k(I_{ij}),$$

which satisfies that: For any $u \in H^2(I_{ij})$ and any $\phi \in Q_k(I_{ij})$:

$$\int_{I_{ij}} \Pi_2 u(x,y)\frac{\partial \phi(x,y)}{\partial x}dxdy = \int_{I_{ij}} u(x,y)\frac{\partial \phi(x,y)}{\partial x}dxdy, \tag{67}$$

$$\int_{J_j} \Pi_2 u\left(x^+_{i-\frac{1}{2}}, y\right)\phi\left(x^+_{i-\frac{1}{2}}, y\right)dy = \int_{J_j} u\left(x^+_{i-\frac{1}{2}}, y\right)\phi\left(x^+_{i-\frac{1}{2}}, y\right)dy. \tag{68}$$

The projection

$$\Pi_3 = P_x^- \otimes P_y^- : H^2(I_{ij}) \to Q_k(I_{ij}),$$

which satisfies that: For any $u \in H^2(I_{ij})$ and any $\phi \in Q_{k-1}(I_{ij})$:

$$\int_{I_{ij}} \Pi_3 u(x,y)\phi(x,y)dxdy = \int_{I_{ij}} u(x,y)\phi(x,y)dxdy, \tag{69}$$

$$\int_{I_i} \Pi_3 u\left(x, y^-_{j+\frac{1}{2}}\right)\phi\left(x, y^-_{j+\frac{1}{2}}\right)dx = \int_{I_i} u\left(x, y^-_{j+\frac{1}{2}}\right)\phi\left(x, y^-_{j+\frac{1}{2}}\right)dx, \tag{70}$$

$$\int_{J_j} \Pi_3 u\left(x^-_{i+\frac{1}{2}}, y\right)\phi\left(x^-_{i+\frac{1}{2}}, y\right)dy = \int_{J_j} u\left(x^-_{i+\frac{1}{2}}, y\right)\phi\left(x^-_{i+\frac{1}{2}}, y\right)dy, \tag{71}$$

$$\Pi_3 u\left(x^-_{i+\frac{1}{2}}, y^-_{j+\frac{1}{2}}\right) = u\left(x^-_{i+\frac{1}{2}}, y^-_{j+\frac{1}{2}}\right). \tag{72}$$

Finally, the usual 2D L_2 projection is denoted as

$$\Pi_4 = P_x \otimes P_y : H^2(I_{ij}) \to Q_k(I_{ij}).$$

The good properties of the projections including the uniqueness and the optimal error estimate can be viewed in lemmas 3.1-3.3 in [33].

The errors between the exact solutions and the numerical solutions can be decomposed by using the above projections:

$$\begin{aligned}
\mathcal{E}_{E_x} &= E_x - E_{xh} = (\Pi_1 E_x - E_{xh}) - (\Pi_1 E_x - E_x) := \ \xi_{E_x} - \eta_{E_x}, \\
\mathcal{E}_{E_y} &= E_y - E_{yh} = (\Pi_2 E_y - E_{yh}) - (\Pi_2 E_y - E_y) := \ \xi_{E_y} - \eta_{E_y}, \\
\mathcal{E}_{D_x} &= D_x - D_{xh} = (\Pi_4 D_x - D_{xh}) - (\Pi_4 D_x - D_x) := \ \xi_{D_x} - \eta_{D_x}, \\
\mathcal{E}_{D_y} &= D_y - D_{yh} = (\Pi_4 D_y - D_{yh}) - (\Pi_4 D_y - D_y) := \ \xi_{D_y} - \eta_{D_y}, \\
\mathcal{E}_H \ &= \ H - H_h \ = \ (\Pi_3 H - H_h) - (\Pi_3 H - H) \ := \ \xi_H - \eta_H,
\end{aligned}$$

Then, following the exact steps in Sect. 3.2.1, and using definitions of the projections (63)-(72) and the property $(\Pi u)_t = \Pi u_t$, we obtain the equation of the errors:

$$\begin{aligned}
&\frac{1}{2}\frac{d}{dt}\Bigg[||\partial_t \xi_{\boldsymbol{D}}||^2 + ||M_C^{\frac{1}{2}}\xi_{\boldsymbol{D}}||^2 + \epsilon_0\lambda_2\left(||M_A^{-\frac{1}{2}}\partial_{t^2}\xi_{\boldsymbol{E}}||^2 + 2\omega_p^2||M_A^{-\frac{1}{2}}\partial_t\xi_{\boldsymbol{E}}||^2 + \omega_p^4||M_A^{-\frac{1}{2}}\xi_{\boldsymbol{E}}||^2\right) \\
&\quad + \mu_0\mu\left(\omega_p^2||\partial_t\xi_H||^2 + ||\partial_{t^2}\xi_H||^2\right)\Bigg] \leq GD + \omega_p^2\left(\sum_{j=1}^{N_y}\mathrm{TEX}_j(\partial_t\eta_H, \partial_t\xi_{E_x}) + \sum_{i=1}^{N_x}\mathrm{TEY}_i(\partial_t\eta_H, \partial_t\xi_{E_y})\right) \\
&\quad + \sum_{j=1}^{N_y}\mathrm{TEX}_j(\partial_{t^2}\eta_H, \partial_{t^2}\xi_{E_x}) + \sum_{i=1}^{Nx}\mathrm{TEY}_i(\partial_{t^2}\eta_H, \partial_{t^2}\xi_{E_y}) \\
&\quad - \omega_p^2\left(\sum_{i=1}^{N_x} c_0\int_{I_i}(\partial_t\xi_{E_x}^+(x, y_{\frac{1}{2}}))^2 + \sum_{j=1}^{N_y} c_0\int_{I_i}(\partial_t\xi_{E_y}^+(x_{\frac{1}{2}}, y))^2\right) \\
&\quad - \left(\sum_{i=1}^{N_x} c_0\int_{I_i}(\partial_{t^2}\xi_{E_x}^+(x, y_{\frac{1}{2}}))^2 + \sum_{j=1}^{N_y} c_0\int_{I_i}(\partial_{t^2}\xi_{E_y}^+(x_{\frac{1}{2}}, y))^2\right).
\end{aligned} \tag{73}$$

The GD, which contains all good terms, is defined as:

$$\begin{aligned}
GD = &-\varepsilon_0\lambda_2\left(M_A^{-1}\partial_{t^2}\eta_{\boldsymbol{E}}, \partial_t\xi_{\boldsymbol{D}}\right) + \varepsilon_0\lambda_2\omega_p^2\left(M_A^{-1}\eta_{\boldsymbol{E}}, \partial_t\xi_{\boldsymbol{D}}\right) + \varepsilon_0\lambda_2\omega_p^2\left(M_A^{-1}\partial_{t^2}\eta_{\boldsymbol{E}}, \partial_t\xi_{\boldsymbol{E}}\right) \\
&+ \varepsilon_0\lambda_2\omega_p^4\left(M_A^{-1}\eta_{\boldsymbol{E}}, \partial_t\xi_{\boldsymbol{E}}\right) + \varepsilon_0\lambda_2\left(M_A^{-1}\partial_{t^3}\eta_{\boldsymbol{E}}, \partial_{t^2}\xi_{\boldsymbol{E}}\right) + \varepsilon_0\lambda_2\omega_p^2\left(M_A^{-1}\partial_t\eta_{\boldsymbol{E}}, \partial_{t^2}\xi_{\boldsymbol{E}}\right) \\
&+ \mu_0\mu\omega_p^2(\partial_{t^2}\eta_H, \partial_t\xi_H) + \mu_0\mu(\partial_{t^3}\eta_H, \partial_{t^2}\xi_H) + \epsilon_0\lambda_2\left(M_A^{-1}\partial_{t^2}\xi_{\boldsymbol{E}} + \omega_p^2 M_A^{-1}\xi_{\boldsymbol{E}}, \partial_t\xi_{\boldsymbol{D}}\right) \\
&+ \left(M_C\partial_t\xi_{\boldsymbol{D}}, \partial_{t^2}\xi_{\boldsymbol{E}}\right) + \omega_p^2\left(M_C\xi_{\boldsymbol{D}}, \partial_t\xi_{\boldsymbol{E}}\right),
\end{aligned} \tag{74}$$

and the terms $\mathrm{TEX}_j(\eta_H, \xi_{E_x})$ and $\mathrm{TEX}_i(\eta_H, \xi_{E_y})$ are defined as

$$\mathrm{TEX}_j = \sum_{i=1}^{N_x}\Bigg(-\int_{I_i}\left(\hat{\eta}_H\xi_{E_x}^-(x, y_{j+\frac{1}{2}}) - \hat{\eta}_H\xi_{E_x}^+(x, y_{j-\frac{1}{2}})\right) + \int_{I_{ij}}\eta_H\partial_y\xi_{E_x}\Bigg), \tag{75}$$

$$\mathrm{TEY}_i = \sum_{j=1}^{N_y}\Big(\int_{I_i}\Big(\hat{\eta}_H\xi^-_{E_y}(x_{i+\frac{1}{2}},y)-\hat{\eta}_H\xi^+_{E_y}(x_{i-\frac{1}{2}},y)\Big)-\int_{I_{ij}}\eta_H\partial_x\xi_{E_y}\Big). \tag{76}$$

By using the following inequalities in [33, Lemmas 3.3-3.4]:

$$\begin{aligned}
&\sum_{j=2}^{N_y}\mathrm{TEX}_j(\eta_H,\xi_{E_x})\le Ch^{2k+2}+\|\xi_{E_x}\|^2,\\
&\sum_{i=2}^{N_x}\mathrm{TEY}_i(\eta_H,\xi_{E_y})\le Ch^{2k+2}+\|\xi_{E_y}\|^2,\\
&\mathrm{TEX}_1(\eta_H,\xi_{E_x})-\sum_{i=1}^{N_x}c_0\int_{I_i}(\xi^+_{E_x}(x,y_{\frac{1}{2}}))^2\le Ch^{2k+2}+\|\xi_{E_x}\|^2,\\
&\mathrm{TEY}_1(\eta_H,\xi_{E_y})-\sum_{j=1}^{N_y}c_0\int_{I_j}(\xi^+_{E_y}(x_{\frac{1}{2}},y))^2\le Ch^{2k+2}+\|\xi_{E_y}\|^2,
\end{aligned} \tag{77}$$

we have

$$RHS\le GD+\omega_p^2(Ch^{2k+2}+C||\partial_t\xi_{\boldsymbol{E}}||^2)+(Ch^{2k+2}+C||\partial_{t^2}\xi_{\boldsymbol{E}}||^2). \tag{78}$$

Applying the Cauchy-Schwarz inequality on the good terms, and using the optimal error estimate of the projections (see lemma 3.3 in [43]), and finally applying the Gronwall inequality and the triangle inequality, we conclude the proof. □

4 The fully-discrete DG method

In this section, we propose the leap-frog DG method to solve the carpet cloak model on unstructured meshes. Before we define the fully-discrete scheme, we introduce the following central difference operators in time: For any time sequence function u^n,

$$\delta_\tau u^{n+\frac{1}{2}}:=\frac{u^{n+1}-u^n}{\tau},\quad \delta_\tau^2u^n:=\frac{\delta_\tau u^{n+\frac{1}{2}}-\delta_\tau u^{n-\frac{1}{2}}}{\tau}=\frac{u^{n+1}-2u^n+u^{n-1}}{\tau^2}.$$

The averaging operators are defined as:

$$\overline{u}^n=\frac{u^{n+1}+u^{n-1}}{2},\quad \breve{u}^n=\frac{u^{n+\frac{1}{2}}+u^{n-\frac{1}{2}}}{2}.$$

Moreover, we need the following discrete Gronwall inequality to prove the discrete stability:

Lemma 4.1. *[41, Lemma. 4.1.2] Assume that the sequence u_n satisfies*

$$u_0\le g_0,\quad \textit{and}\quad u_0\le g_0+r\tau\sum_{s=0}^{n-1}u_s,\ \forall n\ge 1,$$

where g_0, r and τ are some positive constants. Then we have

$$u_n \le g_0 \cdot (1+r\tau)^n \le g_0 \cdot \exp(rn\tau),\ \forall n \ge 1.$$

Now we consider the following leap-frog LDG scheme: For any $n \ge 0$, find D_{xh}^{n+1}, D_{yh}^{n+1}, $H_h^{n+\frac{1}{2}}$, E_{xh}^{n+1}, $E_{yh}^{n+1} \in V_h^k$ such that

$$\int_e \delta_\tau D_{xh}^{n+\frac{1}{2}} \phi_x + \int_e H_h^{n+\frac{1}{2}} \partial_y \phi_x - \int_{\partial e} \hat{H}_h^{n+\frac{1}{2}} \phi_x^{(in)} n_y^{(in)} = 0, \tag{79}$$

$$\int_e \delta_\tau D_{yh}^{n+\frac{1}{2}} \phi_x - \int_e H_h^{n+\frac{1}{2}} \partial_x \phi_y + \int_{\partial e} \hat{H}_h^{n+\frac{1}{2}} \phi_y^{(in)} n_x^{(in)} = 0, \tag{80}$$

$$\varepsilon_0 \lambda_2 \int_e \left(M_A^{-1} \delta_\tau^2 \boldsymbol{E}_h^n + \omega_p^2 M_A^{-1} \overline{\boldsymbol{E}}_h^n \right) \cdot \boldsymbol{u} = \int_e \left(\delta_\tau^2 \boldsymbol{D}_h^n + M_C \overline{\boldsymbol{D}}_h^n \right) \cdot \boldsymbol{u}, \tag{81}$$

$$\mu_0 \mu \int_e \delta_\tau H_h^n \psi - \int_e E_{yh}^n \partial_x \psi + \int_e E_{xh}^n \partial_y \psi + \int_{\partial e} \left(\hat{E}_{yh}^n n_x^{(in)} - \hat{E}_{xh}^n n_y^{(in)} \right) \psi = 0, \tag{82}$$

for all test functions $\phi_x, \phi_y, \boldsymbol{u}, \psi \in V_h^k$, with the following fluxes consistent with (15)-(20):

$$\hat{E}_{xh}^n = E_{xh}^{n,R} \tag{83}$$

$$\hat{E}_{yh}^n = E_{yh}^{n,R} \tag{84}$$

$$\hat{H}_{zh}^{n+\frac{1}{2}} = H_{zh}^{n+\frac{1}{2},L} \tag{85}$$

$$\hat{E}_{xh}^n = 0,\ \text{on } y = c, d \tag{86}$$

$$\hat{E}_{yh}^n = 0,\ \text{on } x = a, b \tag{87}$$

$$\hat{H}_{zh}^{n+\frac{1}{2}} = H_{zh}^{n+\frac{1}{2},(in)},\ \text{on } \partial\Omega. \tag{88}$$

With the above preparation, we can now prove the following energy identity, which is really the discrete form of the energy identity (22).

Theorem 4.2. *For the solution $(\boldsymbol{D}_h^{n+1}, H_h^{n+\frac{1}{2}}, \boldsymbol{E}_h^{n+1})$ of the leap-frog LDG scheme (79)-(82), we define the discrete energy at time level m:*

$$\begin{aligned} ENG_{lf}(m) &= ||\delta_\tau \boldsymbol{D}_h^{m+\frac{1}{2}}||^2 + \frac{1}{2}\left(||M_C^{\frac{1}{2}} \boldsymbol{D}_h^{m+1}||^2 + ||M_C^{\frac{1}{2}} \boldsymbol{D}_h^m||^2 \right) + \varepsilon_0 \lambda_2 ||M_A^{-\frac{1}{2}} \delta_\tau^2 \boldsymbol{E}_h^{m+1}||^2 \\ &+ \frac{\varepsilon_0 \lambda_2 \omega_p^2}{2} \left(3||M_A^{-\frac{1}{2}} \delta_\tau \boldsymbol{E}_h^{m+\frac{1}{2}}||^2 + ||M_A^{-\frac{1}{2}} \delta_\tau \boldsymbol{E}_h^{m-\frac{1}{2}}||^2 \right) + \frac{\varepsilon_0 \lambda_2 \omega_p^4}{2} \left(||M_A^{-\frac{1}{2}} \boldsymbol{E}_h^{m+1}||^2 + ||M_A^{-\frac{1}{2}} \boldsymbol{E}_h^m||^2 \right) \\ &+ \mu_0 \mu \left[\omega_p^2 (\delta_\tau H_h^{m+1}, \delta_\tau H_h^m) + (\delta_\tau^2 H_h^{m+\frac{1}{2}}, \delta_\tau^2 H_h^{m-\frac{1}{2}}) \right]. \end{aligned} \tag{89}$$

Suppose the time step satisfies the constraint:

$$\tau \le \min \left\{ \frac{1}{\sqrt{\varepsilon_0 \lambda_2} \|M_A^{-\frac{1}{2}}\| + \frac{\|M_A^{-\frac{1}{2}} M_B\|}{2\sqrt{\varepsilon_0 \lambda_2}}},\quad \frac{\sqrt{\varepsilon_0 \lambda_2}}{\omega_p \|M_C^{\frac{1}{2}} M_A^{\frac{1}{2}}\|} \right\}, \tag{90}$$

then we have

$$ENG_{lf}(m) \le C \cdot ENG_{lf}(0) \cdot \exp(cm\tau), \qquad \forall m \ge 1, \tag{91}$$

where C and c are positive constants independent of mesh size h and time step τ.

Proof. To make the proof easy to follow, we divide our proof into several major parts.

(I) Choosing $\boldsymbol{u} = \frac{\tau}{2}(\delta_\tau \boldsymbol{D}_h^{n+\frac{1}{2}} + \delta_\tau \boldsymbol{D}_h^{n-\frac{1}{2}}) = \tau \delta_\tau \breve{\boldsymbol{D}}_h^n$ in (81), and using the identity

$$\begin{aligned}\left(M_C \overline{\boldsymbol{D}}_h^n, \frac{\tau}{2}(\delta_\tau \boldsymbol{D}_h^{n+\frac{1}{2}} + \delta_\tau \boldsymbol{D}_h^{n-\frac{1}{2}})\right) &= \left(M_C \frac{\boldsymbol{D}_h^{n+1} + \boldsymbol{D}_h^{n-1}}{2}, \frac{(\boldsymbol{D}_h^{n+1} - \boldsymbol{D}_h^n) + (\boldsymbol{D}_h^n - \boldsymbol{D}_h^{n-1})}{2}\right) \\ &= \frac{1}{4}(||M_C^{\frac{1}{2}} \boldsymbol{D}_h^{n+1}||^2 - ||M_C^{\frac{1}{2}} \boldsymbol{D}_h^{n-1}||^2),\end{aligned} \tag{92}$$

we have

$$\begin{aligned}&\frac{1}{2}(||\delta_\tau \boldsymbol{D}_h^{n+\frac{1}{2}}||^2 - ||\delta_\tau \boldsymbol{D}_h^{n-\frac{1}{2}}||^2) + \frac{1}{4}(||M_C^{\frac{1}{2}} \boldsymbol{D}_h^{n+1}||^2 - ||M_C^{\frac{1}{2}} \boldsymbol{D}_h^{n-1}||^2) \\ &= \tau \varepsilon_0 \lambda_2 \left[(M_A^{-1} \delta_\tau^2 \boldsymbol{E}_h^n, \delta_\tau \breve{\boldsymbol{D}}_h^n) + \omega_p^2 (M_A^{-1} \overline{\boldsymbol{E}}_h^n, \delta_\tau \breve{\boldsymbol{D}}_h^n)\right].\end{aligned} \tag{93}$$

(II) Choosing $\boldsymbol{u} = \frac{\tau}{2}(\delta_\tau \boldsymbol{E}_h^{n+\frac{1}{2}} + \delta_\tau \boldsymbol{E}_h^{n-\frac{1}{2}}) = \tau \delta_\tau \breve{\boldsymbol{E}}_h^n$ in (81), and using the identity

$$\begin{aligned}\left(M_A^{-1} \overline{\boldsymbol{E}}_h^n, \frac{\tau}{2}(\delta_\tau \boldsymbol{E}_h^{n+\frac{1}{2}} + \delta_\tau \boldsymbol{E}_h^{n-\frac{1}{2}})\right) &= \left(M_A^{-1} \frac{\boldsymbol{E}_h^{n+1} + \boldsymbol{E}_h^{n-1}}{2}, \frac{(\boldsymbol{E}_h^{n+1} - \boldsymbol{E}_h^n) + (\boldsymbol{E}_h^n - \boldsymbol{E}_h^{n-1})}{2}\right) \\ &= \frac{1}{4}(||M_A^{-\frac{1}{2}} \boldsymbol{E}_h^{n+1}||^2 - ||M_A^{-\frac{1}{2}} \boldsymbol{E}_h^{n-1}||^2),\end{aligned} \tag{94}$$

we obtain

$$\begin{aligned}&\frac{\varepsilon_0 \lambda_2}{2}(||M_A^{-\frac{1}{2}} \delta_\tau \boldsymbol{E}_h^{n+\frac{1}{2}}||^2 - ||M_A^{-\frac{1}{2}} \delta_\tau \boldsymbol{E}_h^{n-\frac{1}{2}}||^2) + \frac{\varepsilon_0 \lambda_2 \omega_p^2}{4}(||M_A^{-\frac{1}{2}} \boldsymbol{E}_h^{n+1}||^2 - ||M_A^{-\frac{1}{2}} \boldsymbol{E}_h^{n-1}||^2) \\ &= \tau \left(\delta_\tau^2 \boldsymbol{D}_h^n + M_C \overline{\boldsymbol{D}}_h^n, \delta_\tau \breve{\boldsymbol{E}}_h^n\right).\end{aligned} \tag{95}$$

Using (81) to subtract themselves with n replaced by $n-1$, then choosing $\boldsymbol{u} = \frac{1}{2}(\delta_\tau^2 \boldsymbol{E}_h^n + \delta_\tau^2 \boldsymbol{E}_h^{n-1}) = \delta_\tau^2 \breve{\boldsymbol{E}}_h^{n-\frac{1}{2}}$, and using the identity

$$\begin{aligned}&\left(M_A^{-1}(\overline{\boldsymbol{E}}_h^n - \overline{\boldsymbol{E}}_h^{n-1}), \frac{1}{2}(\delta_\tau^2 \boldsymbol{E}_h^n + \delta_\tau^2 \boldsymbol{E}_h^{n-1})\right) \\ &= \left(M_A^{-1} \frac{(\boldsymbol{E}_h^{n+1} + \boldsymbol{E}_h^{n-1}) - (\boldsymbol{E}_h^n + \boldsymbol{E}_h^{n-2})}{2}, \frac{\delta_\tau \boldsymbol{E}_h^{n+\frac{1}{2}} - \delta_\tau \boldsymbol{E}_h^{n-\frac{1}{2}}}{2\tau} + \frac{\delta_\tau \boldsymbol{E}_h^{n+\frac{1}{2}} - \delta_\tau \boldsymbol{E}_h^{n-\frac{3}{2}}}{2\tau}\right) \\ &= \frac{1}{4}\left(M_A^{-1}(\delta_\tau \boldsymbol{E}_h^{n+\frac{1}{2}} + \delta_\tau \boldsymbol{E}_h^{n-\frac{3}{2}}), \delta_\tau \boldsymbol{E}_h^{n+\frac{1}{2}} - \delta_\tau \boldsymbol{E}_h^{n-\frac{3}{2}}\right) \\ &= \frac{1}{4}(||M_A^{-\frac{1}{2}} \delta_\tau \boldsymbol{E}_h^{n+\frac{1}{2}}||^2 - ||M_A^{-\frac{1}{2}} \delta_\tau \boldsymbol{E}_h^{n-\frac{3}{2}}||^2),\end{aligned} \tag{96}$$

we obtain

$$\begin{aligned}&\frac{\varepsilon_0\lambda_2}{2}(||M_A^{-\frac{1}{2}}\delta_\tau^2\boldsymbol{E}_h^n||^2-||M_A^{-\frac{1}{2}}\delta_\tau^2\boldsymbol{E}_h^{n-1}||^2)+\frac{\varepsilon_0\lambda_2\omega_p^2}{4}(||M_A^{-\frac{1}{2}}\delta_\tau\boldsymbol{E}_h^{n+\frac{1}{2}}||^2-||M_A^{-\frac{1}{2}}\delta_\tau\boldsymbol{E}_h^{n-\frac{3}{2}}||^2)\\&=\tau\left(\delta_\tau^3\boldsymbol{D}_h^{n-\frac{1}{2}}+M_C\delta_\tau\overline{\boldsymbol{D}}_h^{n-\frac{1}{2}},\delta_\tau^2\breve{\boldsymbol{E}}_h^{n-\frac{1}{2}}\right).\end{aligned}\tag{97}$$

(III) Multiplying (95) by ω_p^2, and adding the result together with (93) and (97), we have

$$\begin{aligned}&\frac{1}{2}(||\delta_\tau\boldsymbol{D}_h^{n+\frac{1}{2}}||^2-||\delta_\tau\boldsymbol{D}_h^{n-\frac{1}{2}}||^2)+\frac{1}{4}(||M_C^{\frac{1}{2}}\boldsymbol{D}_h^{n+1}||^2-||M_C^{\frac{1}{2}}\boldsymbol{D}_h^{n-1}||^2)\\&+\frac{\varepsilon_0\lambda_2}{2}(||M_A^{-\frac{1}{2}}\delta_\tau^2\boldsymbol{E}_h^{n+1}||^2-||M_A^{-\frac{1}{2}}\delta_\tau^2\boldsymbol{E}_h^{n}||^2)+\frac{\varepsilon_0\lambda_2\omega_p^2}{4}(||M_A^{-\frac{1}{2}}\delta_\tau\boldsymbol{E}_h^{n+\frac{3}{2}}||^2-||M_A^{-\frac{1}{2}}\delta_\tau\boldsymbol{E}_h^{n-\frac{1}{2}}||^2)\\&+\frac{\varepsilon_0\lambda_2\omega_p^2}{2}(||M_A^{-\frac{1}{2}}\delta_\tau\boldsymbol{E}_h^{n+\frac{1}{2}}||^2-||M_A^{-\frac{1}{2}}\delta_\tau\boldsymbol{E}_h^{n-\frac{1}{2}}||^2)+\frac{\varepsilon_0\lambda_2\omega_p^4}{4}(||M_A^{-\frac{1}{2}}\boldsymbol{E}_h^{n+1}||^2-||M_A^{-\frac{1}{2}}\boldsymbol{E}_h^{n-1}||^2)\\&=\tau\varepsilon_0\lambda_2(M_A^{-1}\delta_\tau^2\boldsymbol{E}_h^n+\omega_p^2M_A^{-1}\overline{\boldsymbol{E}}_h^n,\delta_\tau\breve{\boldsymbol{D}}_h^n)\\&\quad+\tau\left(\delta_\tau^3\boldsymbol{D}_h^{n+\frac{1}{2}}+M_C\delta_\tau\overline{\boldsymbol{D}}_h^{n+\frac{1}{2}},\delta_\tau^2\breve{\boldsymbol{E}}_h^{n+\frac{1}{2}}\right)+\tau\omega_p^2\left(\delta_\tau^2\boldsymbol{D}_h^n+M_C\overline{\boldsymbol{D}}_h^n,\delta_\tau\breve{\boldsymbol{E}}_h^n\right).\end{aligned}\tag{98}$$

After dividing both sides of (98) by τ, we can see that (98) is really a discrete form of (28)!

(IV) Similar to the semi-discrete case, now we need to bound the terms $\delta_\tau^3\boldsymbol{D}_h^{n+\frac{1}{2}}$ and $\delta_\tau^2\boldsymbol{D}_h^n$ on the RHS of (98).

Using (79) and (80) to subtract themselves with n replaced by $n-1$, respectively, then letting $\phi_x=\frac{1}{\tau}\delta_\tau\breve{\boldsymbol{E}}_{xh}^n$ and $\phi_y=\frac{1}{\tau}\delta_\tau\breve{\boldsymbol{E}}_{yh}^n$ and adding the results together, we have

$$\begin{aligned}&\int_e\delta_\tau^2\boldsymbol{D}_h^n\cdot\delta_\tau\breve{\boldsymbol{E}}_h^n+\int_e\delta_\tau H_h^n\cdot\partial_y\delta_\tau\breve{E}_{xh}^n-\int_e\delta_\tau H_h^n\cdot\partial_x\delta_\tau\breve{E}_{yh}^n\\&\quad-\int_{\partial e}\delta_\tau\hat{H}_h^n\cdot\delta_\tau\breve{E}_{xh}^{n(in)}n_y^{(in)}+\int_{\partial e}\delta_\tau\hat{H}_h^n\cdot\delta_\tau\breve{E}_{yh}^{n(in)}n_x^{(in)}=0.\end{aligned}\tag{99}$$

Using (82) with n replaced by $n+1$ to subtract itself with n replaced by $n-1$, then choosing $\psi=\frac{1}{2\tau}\delta_\tau H_h^n$, and using the identity

$$E_{yh}^{n+1}-E_{yh}^{n-1}=\tau(\frac{E_{yh}^{n+1}-E_{yh}^n}{\tau}+\frac{E_{yh}^n-E_{yh}^{n-1}}{\tau})=\tau(\delta_\tau E_{yh}^{n+\frac{1}{2}}+\delta_\tau E_{yh}^{n-\frac{1}{2}})=2\tau\delta_\tau\breve{E}_{yh}^n,\tag{100}$$

we have

$$\begin{aligned}&\frac{\mu_0\mu}{2\tau}\int_e(\delta_\tau H_h^{n+1}-\delta_\tau H_h^{n-1})\delta_\tau H_h^n-\int_e\delta_\tau\breve{E}_{yh}^n\cdot\partial_x\delta_\tau H_h^n+\int_e\delta_\tau\breve{E}_{xh}^n\cdot\partial_y\delta_\tau H_h^n\\&\quad+\int_{\partial e}(\delta_\tau\hat{\breve{E}}_{yh}^n n_x^{(in)}-\delta_\tau\hat{\breve{E}}_{xh}^n n_y^{(in)})\delta_\tau H_h^{n(in)}=0.\end{aligned}\tag{101}$$

Adding (99) and (101) together, then using integration by parts, and summing up the result

over all elements, we obtain

$$
\begin{aligned}
&(\delta_\tau^2 \boldsymbol{D}_h^n, \delta_\tau \breve{\boldsymbol{E}}_h^n) + \frac{\mu_0 \mu}{2\tau}(\delta_\tau H_h^{n+1} - \delta_\tau H_h^{n-1}, \delta_\tau H_h^n) + \sum_{e\in\mathcal{T}_h} \int_{\partial e} (-\delta_\tau \hat{H}_h^n \cdot \delta_\tau \breve{E}_{xh}^{n(in)} n_y^{(in)} + \delta_\tau \hat{H}_h^n \cdot \delta_\tau \breve{E}_{yh}^{n(in)} n_x^{(in)}) \\
&+ \sum_{e\in\mathcal{T}_h} \int_{\partial e} (-\delta_\tau H_h^{n(in)} \cdot \delta_\tau \breve{E}_{yh}^{n(in)} n_x^{(in)} + \delta_\tau H_h^{n(in)} \cdot \delta_\tau \breve{E}_{xh}^{n(in)} n_y^{(in)}) \\
&+ \sum_{e\in\mathcal{T}_h} \int_{\partial e} (\delta_\tau \breve{\hat{E}}_{yh}^n n_x^{(in)} - \delta_\tau \breve{\hat{E}}_{xh}^n n_y^{(in)}) \delta_\tau H_h^{n(in)} = 0.
\end{aligned}
\tag{102}
$$

We assign all boundary integral terms of (102) into G_x and G_y classes:

$$
\begin{aligned}
G_x &= \sum_{e\in\mathcal{T}_h} \int_{\partial e} (-\delta_\tau \hat{H}_h^n \cdot \delta_\tau \breve{E}_{xh}^n n_y^{(in)} + \delta_\tau H_h^n \cdot \delta_\tau \breve{E}_{xh}^n n_y^{(in)} - \delta_\tau H_h^n \cdot \delta_\tau \breve{\hat{E}}_{xh}^n n_y^{(in)}), \\
G_y &= \sum_{e\in\mathcal{T}_h} \int_{\partial e} (\delta_\tau \hat{H}_h^n \cdot \delta_\tau \breve{E}_{yh}^n n_x^{(in)} - \delta_\tau H_h^n \cdot \delta_\tau \breve{E}_{yh}^n n_x^{(in)} + \delta_\tau H_h^n \cdot \delta_\tau \breve{\hat{E}}_{yh}^n n_x^{(in)}).
\end{aligned}
\tag{103}
$$

By regrouping terms by sides of the elements and using the definitions of the numerical fluxes $\hat{H}_h^n$ and $\hat{E}_{xh}^n$, we have:

$$
\begin{aligned}
G_x = &\sum_{s\in\mathcal{S}_I} n_y^R \int_s \Big(-\delta_\tau H_h^{n,L} \cdot \delta_\tau \breve{E}_{xh}^{n,R} + \delta_\tau H_h^{n,L} \cdot \delta_\tau \breve{E}_{xh}^{n,L} + \delta_\tau H_h^{n,R} \cdot \delta_\tau \breve{E}_{xh}^{n,R} \\
&-\delta_\tau H_h^{n,L} \cdot \delta_\tau \breve{E}_{xh}^{n,L} - \delta_\tau H_h^{n,R} \cdot \delta_\tau \breve{E}_{xh}^{n,R} + \delta_\tau H_h^{n,L} \cdot \delta_\tau \breve{E}_{xh}^{n,R}\Big) \\
&+ \sum_{s\in\mathcal{S}_{Top}} n_y^R \int_s \Big(-\delta_\tau H_h^{n,(in)} \delta_\tau \breve{E}_{xh}^{n,(in)} + \delta_\tau H_h^{n,(in)} \delta_\tau \breve{E}_{xh}^{n,(in)} - \delta_\tau H_h^{n,(in)} \delta_\tau \breve{\hat{E}}_{xh}^n\Big) \\
&+ \sum_{s\in\mathcal{S}_{Bottom}} n_y^R \int_s \Big(-\delta_\tau H_h^{n,(in)} \delta_\tau \breve{E}_{xh}^{n,(in)} + \delta_\tau H_h^{n,(in)} \delta_\tau \breve{E}_{xh}^{n,(in)} - \delta_\tau H_h^{n,(in)} \delta_\tau \breve{\hat{E}}_{xh}^n\Big) = 0,
\end{aligned}
\tag{104}
$$

where $\mathcal{S}_I$ denotes the set of all non-boundary sides, $\mathcal{S}_{Top}$ represents the set of sides on $y = d$, and $\mathcal{S}_{Bottom}$ on $y = c$.

Similarly, we can prove that $G_y = 0$. Substituting $G_x = G_y = 0$ into (102), we have

$$
(\delta_\tau^2 \boldsymbol{D}_h^n, \delta_\tau \breve{\boldsymbol{E}}_h^n) = -\frac{\mu_0 \mu}{2\tau}(\delta_\tau H_h^{n+1} - \delta_\tau H_h^{n-1}, \delta_\tau H_h^n),
\tag{105}
$$

which is the discrete form of (35).

(V) Following the same technique as (IV), we can obtain

$$
(\delta_\tau^3 \boldsymbol{D}_h^{n-\frac{1}{2}}, \delta_\tau^2 \breve{\boldsymbol{E}}_h^{n-\frac{1}{2}}) = -\frac{\mu_0 \mu}{2\tau}(\delta_\tau^2 H_h^{n+\frac{1}{2}} - \delta_\tau^2 H_h^{n-\frac{3}{2}}, \delta_\tau^2 H_h^{n-\frac{1}{2}}),
\tag{106}
$$

. which is the discrete form of (36).

Substituting (105) and (106) into (98), we have

$$
\begin{aligned}
&\frac{1}{2}(||\delta_\tau \boldsymbol{D}_h^{n+\frac{1}{2}}||^2 - ||\delta_\tau \boldsymbol{D}_h^{n-\frac{1}{2}}||^2) + \frac{1}{4}(||M_C^{\frac{1}{2}} \boldsymbol{D}_h^{n+1}||^2 - ||M_C^{\frac{1}{2}} \boldsymbol{D}_h^{n-1}||^2) \\
&+ \frac{\varepsilon_0\lambda_2}{2}(||M_A^{-\frac{1}{2}}\delta_\tau^2 \boldsymbol{E}_h^n||^2 - ||M_A^{-\frac{1}{2}}\delta_\tau^2 \boldsymbol{E}_h^{n-1}||^2) + \frac{\varepsilon_0\lambda_2\omega_p^2}{4}(||M_A^{-\frac{1}{2}}\delta_\tau \boldsymbol{E}_h^{n+\frac{1}{2}}||^2 - ||M_A^{-\frac{1}{2}}\delta_\tau \boldsymbol{E}_h^{n-\frac{3}{2}}||^2) \\
&+ \frac{\varepsilon_0\lambda_2\omega_p^2}{2}(||M_A^{-\frac{1}{2}}\delta_\tau \boldsymbol{E}_h^{n+\frac{1}{2}}||^2 - ||M_A^{-\frac{1}{2}}\delta_\tau \boldsymbol{E}_h^{n-\frac{1}{2}}||^2) + \frac{\varepsilon_0\lambda_2\omega_p^4}{4}(||M_A^{-\frac{1}{2}} \boldsymbol{E}_h^{n+1}||^2 - ||M_A^{-\frac{1}{2}} \boldsymbol{E}_h^{n-1}||^2) \\
&+ \frac{\mu_0\mu}{2}\left[\omega_p^2(\delta_\tau H_h^{n+1} - \delta_\tau H_h^{n-1}, \delta_\tau H_h^n) + (\delta_\tau^2 H_h^{n+\frac{1}{2}} - \delta_\tau^2 H_h^{n-\frac{3}{2}}, \delta_\tau^2 H_h^{n-\frac{1}{2}})\right] \\
&= \tau\varepsilon_0\lambda_2(M_A^{-1}\delta_\tau^2 \boldsymbol{E}_h^n + \omega_p^2 M_A^{-1}\overline{\boldsymbol{E}}_h^n, \delta_\tau \breve{\boldsymbol{D}}_h^n) + \tau\left(M_C\delta_\tau \overline{\boldsymbol{D}}_h^{n-\frac{1}{2}}, \delta_\tau^2 \breve{\boldsymbol{E}}_h^{n-\frac{1}{2}}\right) + \tau\omega_p^2\left(M_C\overline{\boldsymbol{D}}_h^n, \delta_\tau \breve{\boldsymbol{E}}_h^n\right),
\end{aligned}
\tag{107}
$$

which is the discrete form of (37).

Multiplying (107) by 2, then summing up the result from $n = 1$ to $n = m$, and using the identity

$$
\sum_{n=1}^{m}(a_{n+1} - a_{n-1}, a_n) = (a_{m+1}, a_m) - (a_1, a_0), \tag{108}
$$

we obtain

$$
\begin{aligned}
ENG_{LF}(m) - ENG_{LF}(0) = \sum_{n=1}^{m} 2\Big[&\tau\varepsilon_0\lambda_2(M_A^{-1}\delta_\tau^2 \boldsymbol{E}_h^n + \omega_p^2 M_A^{-1}\overline{\boldsymbol{E}}_h^n, \delta_\tau \breve{\boldsymbol{D}}_h^n) \\
&+ \tau(M_C\delta_\tau \overline{\boldsymbol{D}}_h^{n-\frac{1}{2}}, \delta_\tau^2 \breve{\boldsymbol{E}}_h^{n-\frac{1}{2}}) + \tau\omega_p^2(M_C\overline{\boldsymbol{D}}_h^n, \delta_\tau \breve{\boldsymbol{E}}_h^n)\Big].
\end{aligned}
\tag{109}
$$

Then, we just need to bound the RHS terms of (109) and use the lemma. 4.1 to finish the proof. By using the following two inequalities and estimating the RHS terms one by one:

$$
2ab \le a^2 + b^2, \qquad \left(\frac{a+b}{2}\right)^2 \le \frac{1}{2}(a+b)^2,
$$

we obtain the following four estimates:

$$
\begin{aligned}
&\sum_{n=1}^{m} 2\tau\varepsilon_0\lambda_2(M_A^{-1}\delta_\tau^2 \boldsymbol{E}_h^n, \delta_\tau \breve{\boldsymbol{D}}_h^n) \le \sum_{n=1}^{m} 2\tau\varepsilon_0\lambda_2\|M_A^{-\frac{1}{2}}\|\|M_A^{-\frac{1}{2}}\delta_\tau^2 \boldsymbol{E}_h^n\|\|\frac{1}{2}\delta_\tau(\boldsymbol{D}_h^{n+\frac{1}{2}} + \boldsymbol{D}_h^{n-\frac{1}{2}})\| \\
&\le \tau\sqrt{\varepsilon_0\lambda_2}\|M_A^{-\frac{1}{2}}\| \sum_{n=1}^{m}\left(\varepsilon_0\lambda_2\|M_A^{-\frac{1}{2}}\delta_\tau^2 \boldsymbol{E}_h^n\|^2 + \frac{1}{2}(\|\delta_\tau \boldsymbol{D}_h^{n+\frac{1}{2}}\|^2 + \|\delta_\tau \boldsymbol{D}_h^{n-\frac{1}{2}}\|^2)\right),
\end{aligned}
\tag{110}
$$

$$
\begin{aligned}
&\sum_{n=1}^{m} 2\tau\varepsilon_0\lambda_2\omega_p^2(M_A^{-1}\overline{\boldsymbol{E}}_h^n, \delta_\tau\breve{\boldsymbol{D}}_h^n)\\
&\le \sum_{n=1}^{m} 2\tau\varepsilon_0\lambda_2\omega_p^2\|M_A^{-\frac{1}{2}}\|\|M_A^{-\frac{1}{2}}\frac{1}{2}(\boldsymbol{E}_h^{n+1}+\boldsymbol{E}_h^{n-1})\|\|\frac{1}{2}\delta_\tau(\boldsymbol{D}_h^{n+\frac{1}{2}}+\boldsymbol{D}_h^{n-\frac{1}{2}})\|\\
&\le \tau\sqrt{\varepsilon_0\lambda_2}\|M_A^{-\frac{1}{2}}\|\sum_{n=1}^{m} 2\sqrt{\varepsilon_0\lambda_2}\omega_p^2\|\frac{1}{2}(M_A^{-\frac{1}{2}}\boldsymbol{E}_h^{n+1}+M_A^{-\frac{1}{2}}\boldsymbol{E}_h^{n-1})\|\cdot\|\frac{1}{2}\delta_\tau(\boldsymbol{D}_h^{n+\frac{1}{2}}+\boldsymbol{D}_h^{n-\frac{1}{2}})\|\\
&\le \tau\sqrt{\varepsilon_0\lambda_2}\|M_A^{-\frac{1}{2}}\|\sum_{n=1}^{m}\bigg(\frac{\varepsilon_0\lambda_2\omega_p^4}{2}(\|M_A^{-\frac{1}{2}}\boldsymbol{E}_h^{n+1}\|^2+\|M_A^{-\frac{1}{2}}\boldsymbol{E}_h^{n-1}\|^2)+\frac{1}{2}(\|\delta_\tau\boldsymbol{D}_h^{n+\frac{1}{2}}\|^2+\|\delta_\tau\boldsymbol{D}_h^{n-\frac{1}{2}}\|^2)\bigg),
\end{aligned}
\tag{111}
$$

$$
\begin{aligned}
&\sum_{n=1}^{m} 2\tau(M_C\delta_\tau\overline{\boldsymbol{D}}_h^{n-\frac{1}{2}}, \delta_\tau^2\breve{\boldsymbol{E}}_h^{n-\frac{1}{2}}) = \sum_{n=1}^{m} 2\tau\bigg(M_A^{-1}M_B\cdot\frac{1}{2}\delta_\tau(\boldsymbol{D}_h^{n+\frac{1}{2}}+\boldsymbol{D}_h^{n-\frac{3}{2}}), \frac{1}{2}\delta_\tau^2(\boldsymbol{E}_h^n+\boldsymbol{E}_h^{n-1})\bigg)\\
&\le \sum_{n=1}^{m}\frac{\tau\|M_A^{-\frac{1}{2}}M_B\|}{\sqrt{\varepsilon_0\lambda_2}}\cdot 2\|\frac{1}{2}\delta_\tau(\boldsymbol{D}_h^{n+\frac{1}{2}}+\boldsymbol{D}_h^{n-\frac{3}{2}})\|\cdot\sqrt{\varepsilon_0\lambda_2}\|M_A^{-\frac{1}{2}}\frac{1}{2}\delta_\tau^2(\boldsymbol{E}_h^n+\boldsymbol{E}_h^{n-1})\|\\
&\le \frac{\tau\|M_A^{-\frac{1}{2}}M_B\|}{\sqrt{\varepsilon_0\lambda_2}}\sum_{n=1}^{m}\frac{1}{2}(\|\delta_\tau\boldsymbol{D}_h^{n+\frac{1}{2}}\|^2+\|\delta_\tau\boldsymbol{D}_h^{n-\frac{3}{2}}\|^2)+\frac{\varepsilon_0\lambda_2}{2}(\|M_A^{-\frac{1}{2}}\delta_\tau^2\boldsymbol{E}_h^n\|^2+\|M_A^{-\frac{1}{2}}\delta_\tau^2\boldsymbol{E}_h^{n-1}\|^2),
\end{aligned}
\tag{112}
$$

and

$$
\begin{aligned}
&\sum_{n=1}^{m} 2\tau\omega_p^2(M_C\overline{\boldsymbol{D}}_h^n, \delta_\tau\breve{\boldsymbol{E}}_h^n) = \sum_{n=1}^{m} 2\tau\omega_p^2\bigg(M_C^{\frac{1}{2}}\frac{1}{2}(\boldsymbol{D}_h^{n+1}+\boldsymbol{D}_h^{n-1}), M_C^{\frac{1}{2}}M_A^{\frac{1}{2}}M_A^{-\frac{1}{2}}\frac{1}{2}\delta_\tau(\boldsymbol{E}_h^{n+\frac{1}{2}}+\boldsymbol{E}_h^{n-\frac{1}{2}})\bigg)\\
&\le \frac{\tau\omega_p\|M_C^{\frac{1}{2}}M_A^{\frac{1}{2}}\|}{\sqrt{\varepsilon_0\lambda_2}}\sum_{n=1}^{m} 2\|M_C^{\frac{1}{2}}\frac{1}{2}(\boldsymbol{D}_h^{n+1}+\boldsymbol{D}_h^{n-1})\|\cdot\sqrt{\varepsilon_0\lambda_2}\omega_p\|M_A^{-\frac{1}{2}}\frac{1}{2}\delta_\tau(\boldsymbol{E}_h^{n+\frac{1}{2}}+\boldsymbol{E}_h^{n-\frac{1}{2}})\|\\
&\le \frac{\tau\omega_p\|M_C^{\frac{1}{2}}M_A^{\frac{1}{2}}\|}{\sqrt{\varepsilon_0\lambda_2}}\sum_{n=1}^{m}\frac{1}{2}(\|M_C^{\frac{1}{2}}\boldsymbol{D}_h^{n+1}\|^2+\|M_C^{\frac{1}{2}}\boldsymbol{D}_h^{n-1})\|^2)+\frac{\varepsilon_0\lambda_2\omega_p^2}{2}(\|M_A^{-\frac{1}{2}}\delta_\tau\boldsymbol{E}_h^{n+\frac{1}{2}}\|^2+\|M_A^{-\frac{1}{2}}\delta_\tau\boldsymbol{E}_h^{n-\frac{1}{2}}\|^2)
\end{aligned}
\tag{113}
$$

Substituting (110)-(113) into (109), and choosing the time step τ to make the coefficients of $\|M_C^{\frac{1}{2}}\boldsymbol{D}_h^{n+1}\|$, $\|\delta_\tau\boldsymbol{D}_h^{n+\frac{1}{2}}\|$, $\|M_A^{-\frac{1}{2}}\boldsymbol{E}_h^{n+1}\|$, $\|M_A^{-\frac{1}{2}}\delta_\tau\boldsymbol{E}_h^{n+\frac{1}{2}}\|$, on the LHS smaller than those on the RHS:

$$
\frac{\tau\omega_p\|M_C^{\frac{1}{2}}M_A^{\frac{1}{2}}\|}{2\sqrt{\varepsilon_0\lambda_2}}\le\frac{1}{2},\quad \tau\sqrt{\varepsilon_0\lambda_2}\|M_A^{-\frac{1}{2}}\|+\frac{\tau\|M_A^{-\frac{1}{2}}M_B\|}{2\sqrt{\varepsilon_0\lambda_2}}\le 1,\quad \tau\sqrt{\varepsilon_0\lambda_2}\|M_A^{-\frac{1}{2}}\|\le 1,\quad \frac{\tau\omega_p\|M_C^{\frac{1}{2}}M_A^{\frac{1}{2}}\|}{\sqrt{\varepsilon_0\lambda_2}}\le 3,
$$

which is equivalent to (90). Finally by applying the discrete Gronwall inequality given in lemma.4.1, we finish the proof. □

5 Numerical results

In this section, we present two accuracy tests of the leap-frog DG methods (79)-(82) on the rectangular mesh and unstructured mesh, to verify the proved convergence results. Additionally, some numerical simulations of the cloaking phenomenon will be shown.

5.1 The error table on triangular meshes

We use the model in [34, Sect. 5] to test the convergence rate of our model:

$$\partial_t D_x = \frac{\partial H}{\partial y}, \tag{114}$$

$$\partial_t D_y = -\frac{\partial H}{\partial x}, \tag{115}$$

$$\varepsilon_0\lambda_2\left(M_A^{-1}\partial_{t^2}\boldsymbol{E} + \omega_p^2 M_A^{-1}\boldsymbol{E}\right) = \partial_{t^2}\boldsymbol{D} + M_C\boldsymbol{D} + \boldsymbol{f}(t_n), \tag{116}$$

$$\mu_0\mu\partial_t H = -\nabla\times\boldsymbol{E}, \tag{117}$$

where the source term $\boldsymbol{f}$ is

$$\boldsymbol{f}(x,y,t) = \varepsilon_0\lambda_2\left(M_A^{-1}\partial_{t^2}\boldsymbol{E} + \omega_p^2 M_A^{-1}\boldsymbol{E}\right) - \partial_{t^2}\boldsymbol{D} - M_C\boldsymbol{D}. \tag{118}$$

The model has exact solutions

$$E_x(x,y,t) = \cos(\omega x)\sin(\omega y)e^{-\omega_f t}, \tag{119}$$

$$E_y(x,y,t) = -\sin(\omega x)\cos(\omega y)e^{-\omega_f t}, \tag{120}$$

$$D_x(x,y,t) = \frac{-2\omega}{\mu_0\mu\omega_f^2}\cos(\omega x)\sin(\omega y)e^{-\omega_f t}, \tag{121}$$

$$D_y(x,y,t) = \frac{-2\omega}{\mu_0\mu\omega_f^2}(-\sin(\omega x)\cos(\omega y))e^{-\omega_f t}, \tag{122}$$

$$H(x,y,t) = \frac{-2\omega}{\mu_0\mu\omega_f}\cos(\omega x)\cos(\omega y)e^{-\omega_f t}. \tag{123}$$

We use the unit square as our physical domain, which is partitioned by the triangular mesh. Fig. 2 shows a sample coarse mesh.

We couple the leap-frog time discretization with the second and third order DG methods, and apply the alternating fluxes and the PEC boundary conditions (83)-(88) to solve the model. The physical parameters in the test are chosen as:

$$H_1 = 0.05,\quad H_2 = 0.2,\quad d = 0.2,\quad \epsilon_0 = \mu_0 = \pi,\quad \mu = 4\pi,\quad T = 0.1.$$

The time step is chosen as $\tau = 0.01h$ for the second order DG method, and $\tau = 0.01h^{\frac{3}{2}}$ for the third order DG method, where h is the mesh size. The L_2 errors and the corresponding convergence rates of $||\boldsymbol{E}_h^{n+1} - \boldsymbol{E}(t_{n+1})||$, $||\boldsymbol{D}_h^{n+1} - \boldsymbol{D}(t_{n+1})||$, and $||H_h^{n+\frac{1}{2}} - H(t_{n+\frac{1}{2}})||$ are shown in Table 1. We observe the sub-optimal convergence rates of $O(h^p)$ in the L^2 norm, which is consistent with Theorem 3.2.

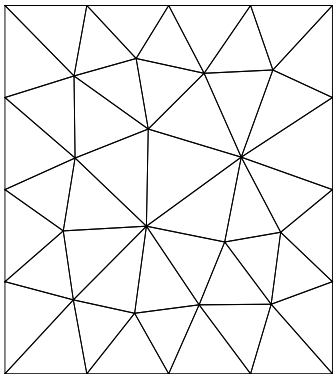

Figure 2: Sample mesh for the unit region.

Table 1: L_2 errors and orders obtained the DG method for $\boldsymbol{E}$,$\boldsymbol{D}$, and H on the unstructured mesh.

	k=1					
Level of refinement	$\boldsymbol{E}$ error	order	$\boldsymbol{D}$ error	order	H error	order
1	1.15 E-01		5.31 E-01		9.91 E-02	
2	4.17 E-02	1.29	2.09 E-01	1.34	3.06 E-02	1.69
3	1.38 E-02	1.77	5.98 E-02	1.80	1.33 E-02	1.19
4	4.67 E-03	1.56	1.88 E-02	1.66	2.49 E-03	2.42
5	2.24 E-03	1.05	8.69 E-03	1.11	6.63 E-04	1.91
	k=2					
Level of refinement	$\boldsymbol{E}$ error	order	$\boldsymbol{D}$ error	order	H error	order
1	2.66 E-02		1.21 E-01		1.99 E-02	
2	4.60 E-03	2.53	2.07 E-02	2.54	3.49 E-03	2.51
3	7.31 E-04	2.65	3.11 E-03	2.73	4.71 E-04	2.88
4	1.27 E-04	2.51	4.90 E-04	2.66	6.68 E-05	2.82
5	2.82 E-05	2.17	1.5 E-04	2.21	9.10 E-06	2.87

Table 2: L_2 errors and orders obtained from the leap-frog DG method for $\boldsymbol{E}$,$\boldsymbol{D}$, and H on the rectangular mesh.

	k=1					
# cells	$\boldsymbol{E}$ error	order	$\boldsymbol{D}$ error	order	H error	order
10×10	1.38 E-02		8.98 E-02		1.38 E-02	
20×20	3.40 E-03	1.95	2.26 E-02	1.96	3.40 E-03	1.95
40×40	8.67 E-04	1.97	5.73 E-03	1.98	8.67 E-04	1.97
80×80	2.18 E-04	1.99	1.43 E-03	1.99	2.18 E-04	1.99
160×160	5.47 E-05	2.00	3.60 E-04	1.99	5.47 E-05	2.00
	k=2					
# cells	$\boldsymbol{E}$ error	order	$\boldsymbol{D}$ error	order	H error	order
10×10	7.93 E-03		2.18 E-02		6.57 E-03	
20×20	9.85 E-04	3.00	2.75 E-03	2.98	8.41 E-04	2.96
40×40	1.22 E-04	3.01	3.47 E-04	2.98	1.10 E-04	2.97
80×80	1.52 E-05	3.00	4.33 E-05	2.99	1.37 E-05	3.01
160×160	1.90 E-06	3.00	5.42 E-06	2.99	1.71 E-06	3.00

5.2 The error table on rectangular meshes

Next, we partition the unit square domain with the rectangular mesh, and apply the alternating fluxes with additional jump terms on the PEC boundary conditions (54)-(61) to simulate the model (114)-(117). To achieve the optimal order of convergence, we set the initial conditions as:

$$E_{xh}(0) = \Pi_1 E_x(0),\ \ E_{yh}(0) = \Pi_2 E_y(0),\ \ D_{xh}(0) = \Pi_4 D_x(0),\ \ D_{yh}(0) = \Pi_4 D_y(0),\ \ H_h(0) = \Pi_3 H(0).$$

Table. 2 shows the L^2 errors and the convergence rates in this case. As proved in Theorem 3.3, the optimal order of accuracy is obtained.

5.3 The wave propagation cross the cloaking region

To see the invisibility cloaking phenomenon, we test our leap-frog DG scheme on Example 2 in [34], where the physical domain is $[-0.6, 0.6]\text{m} \times [0, 0.6]\text{m}$, and the physical parameters for the simulation are

$$H_1 = 0.1m, \quad H_2 = 0.4m, \quad d = 0.4m, \quad \tau = 1e-13s.$$

The domain is partitioned by the unstructured triangular mesh with mesh size $h = 0.01$m, and it is surrounded by a perfectly matched layer (PML) of thickness $15h$ to absorb outgoing waves. In this paper, we use the classical 2D Berenger PML, whose governing equations are [30]:

$$\epsilon_0 \partial_t \boldsymbol{E} + \begin{pmatrix} \sigma_y & 0 \\ 0 & \sigma_x \end{pmatrix} \boldsymbol{E} = \nabla \times H_z, \tag{124}$$

$$\mu_0 \partial_t H_{zx} + \sigma_{mx} H_{zx} = -\frac{\partial E_y}{\partial x}, \tag{125}$$

$$\mu_0 \partial_t H_{zy} + \sigma_{my} H_{zy} = \frac{\partial E_x}{\partial y}, \tag{126}$$

where $H_z = H_{zx} + H_{zy}$ represents the magnetic field, and we denote the parameters σ_i and $\sigma_{m,i}$, $i = x, y$ as the electric and the magnetic conductivities in the x- and y- directions respectively.

In the domain, an incident Gaussian wave

$$H(x, y, t) = \sin(2\pi f) \exp(-\frac{|\boldsymbol{x} - \boldsymbol{x}_c|^2}{L^2})$$

is imposed along a line segment with endpoints $(-d, d/2)$ and $(-d/2, d)$. We set the frequency $f = 2\text{GHz}$, $L = 0.25\sqrt{2}d$, and $\boldsymbol{x}_c = (-3d/4, 3d/4)$, where $\boldsymbol{x} = (x, y)$ is an arbitrary point on the segment. The Fig. 3 shows that the computational domain is wrapped by the green PML region. The red quadrilateral region represents the cloaking region, where the carpet cloak model (1-4) is solved. The rest blue region is vacuum, where the standard Maxwell equation is solved. The numerical magnetic field H at different time steps are shown in Fig. 4, and it can be observed that the wave looks like the one reflecting from the flat ground, and the the hidden region is invisible to the observers at the far end.

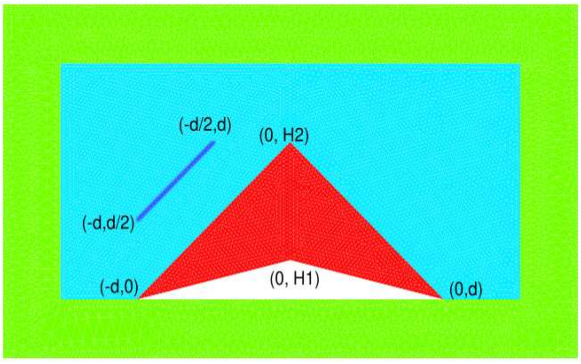

Figure 3: The computational domain for Examples 5.3 and 5.4.

For the comparison, the simulation of the magnetic field H without the cloaking material is presented in Fig. 5, and the cloak phenomenon disappears in this case.

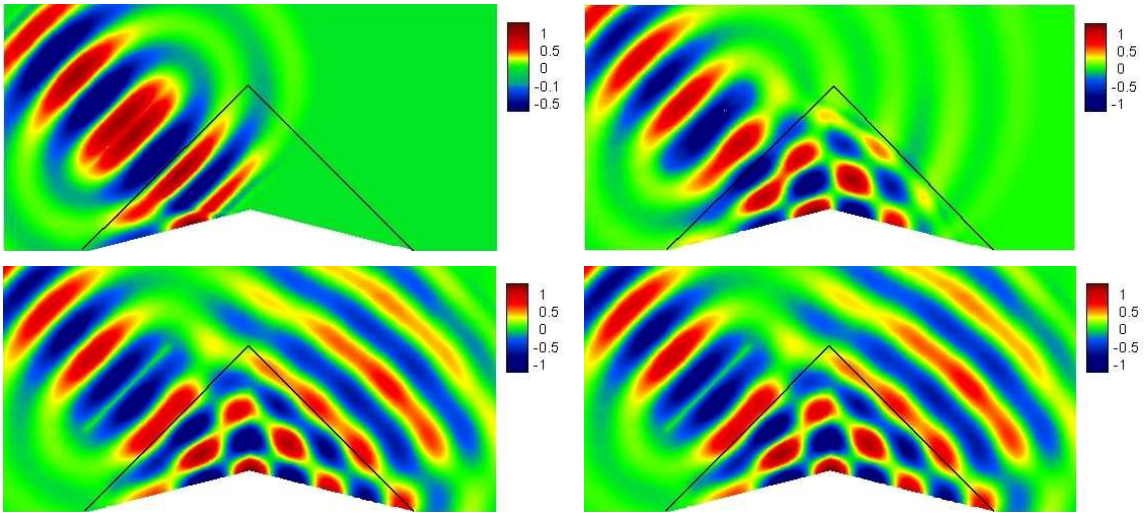

Figure 4: Example 5.3 (with metamaterial). The magnetic field H obtained at 12000, 24000, 40000, and 50000 time steps (oriented counterclockwise).

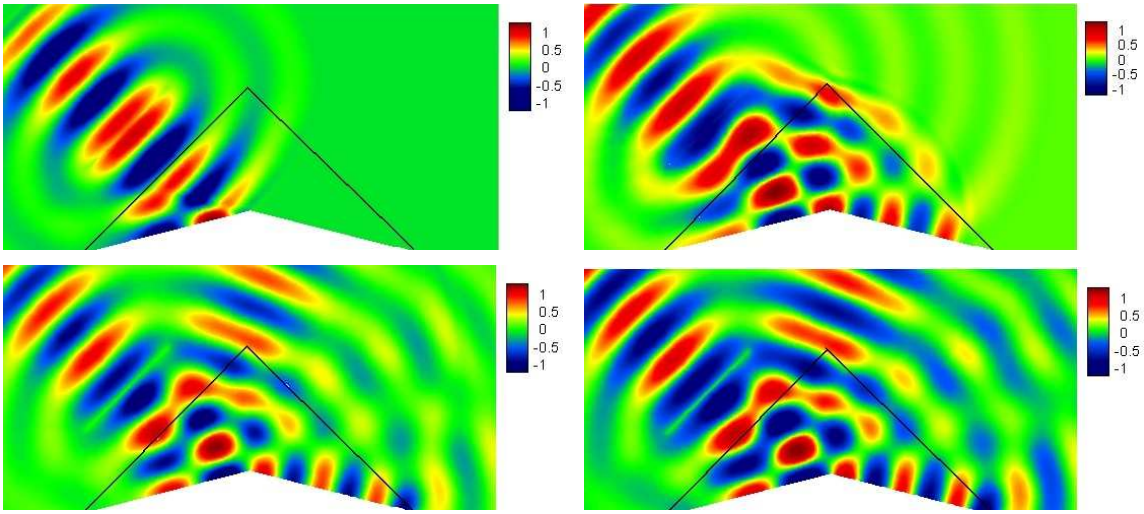

Figure 5: Example 5.3 (without metamaterial). The magnetic field H obtained at 12000, 24000, 40000, and 50000 time steps (oriented counterclockwise).

5.4 The wave propagation with a vertical incident wave source

We repeat Example 5.2, and substitute the incident Gaussian wave to a vertical source wave $H(x, y, t) = 0.1 \sin(2\pi f)$ with the frequency $f = 2\text{GHz}$ on edge $x = -0.6\text{m}$. The numerical solutions of H at each time step are shown in Fig. 6. This result shows that the plane wave pattern is perfectly recovered after passing through the cloaking region, and we conclude that the cloaking phenomenon is also achieved in this case.

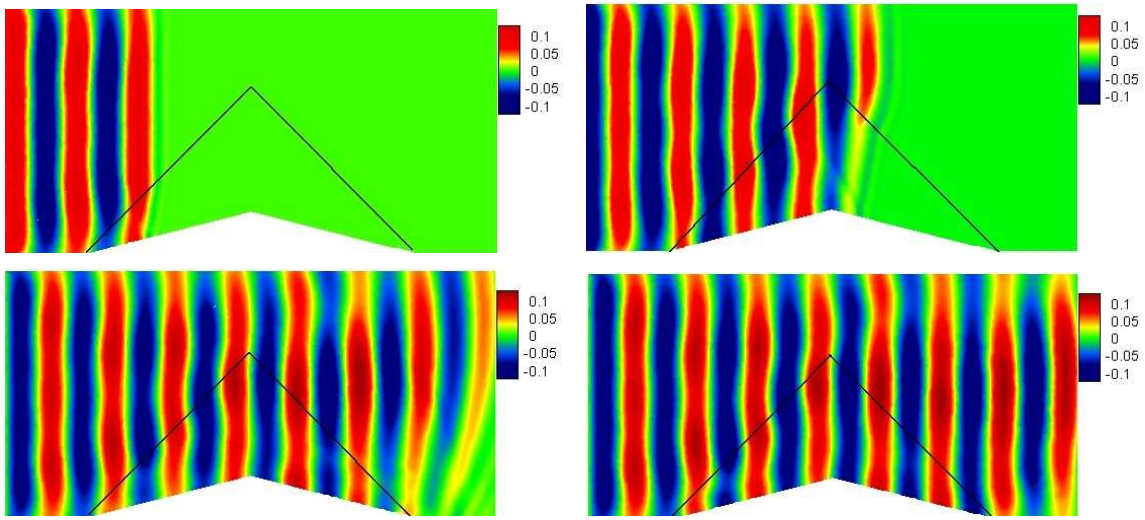

Figure 6: Example 5.4. The magnetic field H obtained at 12000, 24000,40000, and 50000 time steps (oriented counterclockwise).

6 Conclusion

In this paper, we develop the leap-frog DG scheme for solving the time-domain carpet cloak model. We prove the stability and the sub-optimal order of convergence for the semi-discrete scheme on triangular meshes, and the optimal order of convergence on rectangular meshes with tensor-product DG spaces. Then, the conditional stability for the fully-discrete scheme with the time step constraint $\tau = O(h)$ is proved. Numerically, the sub-optimal convergence rate on unstructured meshes and the optimal convergence rate on rectangular meshes with tensor-product DG spaces are verified in the error accuracy tests. Moreover, simulations of wave propagation in the carpet cloak region are presented.

References

[1] H. Ammari, H. Kang, H. Lee, M. Lim and S. Yu, Enhancement of near cloaking for the full Maxwell equations, SIAM J. Appl. Math. 73 (2013) 2055-2076.

[2] A. Anees and L. Angermann, Time domain finite element method for Maxwell's equations, IEEE Access, 7 (2019) 63852-63867.

[3] V.A. Bokil, Y. Cheng, Y. Jiang and F.Li, Energy stable discontinuous Galerkin methods for Maxwell's equations in nonlinear optical media. J. Comput. Phys. 350 (2017) 420-452.

[4] S.C. Brenner, J. Gedicke and L.-Y. Sung, An adaptive P1 finite element method for two-dimensional transverse magnetic time harmonic Maxwell's equations with general material properties and general boundary conditions, J. Sci. Comput. 68 (2016) 848-863.
[5] A. Buffa, P. Houston and I. Perugia, Discontinuous Galerkin computation of the Maxwell eigenvalues on simplicial meshes, J. Comput. Appl. Math. 204 (2007) 317-333.
[6] M. Cassier, P. Joly and M. Kachanovska, Mathematical models for dispersive electromagnetic waves: An overview, Comput. Math. Appl. 74 (2017) 2792-2830.
[7] E.T. Chung, P.Ciarlet Jr., T.F. Yu, Convergence and superconvergence of staggered discontinuous Galerkin methods for the three-dimensional Maxwell equations on Cartesian grids, J. Comput. Phys. 235 (2013) 14–31.
[8] E.T. Chung and P. Ciarlet Jr., A staggered discontinuous Galerkin method for wave propagation in media with dielectrics and meta-materials, J. Comput. Appl. Math. 239 (2013) 189-207.
[9] P.G. Ciarlet, Finite Element Method for Elliptic Problems. SIAM, Philadelphia, 2002.
[10] B.Cockburn, F.Li, C.-W.Shu, Locally divergence-free discontinuous Galerkin methods for the Maxwell equations, J. Comput. Phys. 194 (2004) 588–610.
[11] B. Cockburn and C.-W. Shu, TVB Runge-Kutta local projection discontinuous Galerkin finite element method for conservation laws II: general framework, Math. Comp. 52 (1989) 411-435.
[12] B. Cockburn and C.-W. Shu, The Runge-Kutta discontinuous Galerkin method for conservation laws V: multidimensional systems, J. Comput. Phys. 141 (1998) 199-224.
[13] B. Cockburn and C.-W. Shu, The local discontinuous Galerkin method for time-dependent convection-diffusion systems, SIAM J. Numer. Anal. 35 (1998) 2240-2463.
[14] B. Cockburn and C.-W. Shu, Runge-Kutta discontinuous Galerkin methods for convection-dominated problems, J. Sci. Comput. 16 (2001) 173-261.
[15] L. Demkowicz, J. Kurtz, D. Pardo, M. Paszynski, W. Rachowicz and A. Zdunek, Computing with hp-Adaptive Finite Elements. Vol.2: Frontiers: Three Dimensional Elliptic and Maxwell Problems with Applications. Chapman & Hall/CRC, 2008.
[16] L. Fezoui, S. Lanteri, S. Lohrengel, S. Piperno, Convergence and stability of a discontinuous Galerkin time-domain method for the 3D heterogeneous Maxwell equations on unstructured meshes, Model. Math. Anal. Numer. 39 (2005) 1149–1176.
[17] A. Greenleaf, Y. Kurylev, M. Lassas and G. Uhlmann, Cloaking devices, electromagnetics wormholes and transformation optics, SIAM Review 51 (2009) 3-33.
[18] F. Guevara Vasquez, G.W. Milton and D. Onofrei, Broadband exterior cloaking, Opt. Express 17 (2009) 14800-14805.
[19] Y. Hao and R. Mittra, FDTD Modeling of Metamaterials: Theory and Applications, Artech House Publishers, 2008.
[20] J.S. Hesthaven and T. Warburton, Nodal Discontinuous Galerkin Methods: Algorithms, Analysis, and Applications. Springer, New York, 2008.
[21] R. Hiptmair, Finite elements in computational electromagnetism, Acta Numerica 11 (2002) 237-339.
[22] J. Hong, L. Ji and L. Kong, Energy-dissipation splitting finite-difference time-domain method for Maxwell equations with perfectly matched layers, J. Comput. Phys. 269 (2014) 201-214.
[23] R.V. Kohn, D. Onofrei, M.S. Vogelius and M.I. Weinstein, Cloaking via change of variables for the Helmholtz equation, Comm. Pure Appl. Math. 63 (2010) 973-1016.
[24] S. Lanteri, C. Scheid, Convergence of a discontinuous Galerkin scheme for the mixed time domain Maxwells equations in dispersive media, IMA J. Numer. Anal. 33 (2013) 432–459.

[25] J.J. Lee, A mixed method for time-transient acoustic wave propagation in metamaterials, J. Sci. Comput. (2020) 84:20.
[26] U. Leonhardt, Optical conformal mapping, Science 312 (2006) 1777-1780.
[27] J. Li, Development of discontinuous Galerkin methods for Maxwell's equations in metamaterials and perfectly matched layers, J. Comput. Appl. Math. 236 (2011) 950–961.
[28] J. Li and J.S. Hesthaven, Analysis and application of the nodal discontinuous Galerkin method for wave propagation in metamaterials, J. Comput. Phys. 258 (2014) 915-930.
[29] J. Li and Y. Huang, Time-Domain Finite Element Methods for Maxwell's Equations in Metamaterials. Springer Berlin Heidelberg, 2013.
[30] J. Li, Y. Huang and W. Yang, Well-posedness study and finite element simulation of time-domain cylindrical and elliptical cloaks, Math. Comp. 84 (2015) 543-562.
[31] J. Li, Y. Huang, W. Yang and A. Wood, Mathematical analysis and time-domain finite element simulation of carpet cloak, SIAM J. Appl. Math. 74(4) (2014) 1136-1151.
[32] J. Li, C. Meng and Y. Huang, Improved analysis and simulation of a time-domain carpet cloak model, Comput. Methods Appl. Math. 19(2) (2019) 359-378.
[33] J. Li, C. Shi and C.-W. Shu, Optimal non-dissipative discontinuous Galerkin methods for Maxwell's equations in Drude metamaterials, Comput. Math. Appl. 73 (2017) 1768-1780.
[34] J. Li, C.-W. Shu and W. Yang, Development and analysis of two new finite element schemes for a time-domain carpet cloak model, Adv. Comput. Math., submitted.
[35] J. Li, J.W. Waters and E.A. Machorro, An implicit leap-frog discontinuous Galerkin method for the time-domain Maxwell's equations in metamaterials, Comput. Methods Appl. Mech. Engrg. 223-224 (2012) 43–54.
[36] W. Li, D. Liang and Y. Lin, Symmetric energy-conserved S-FDTD scheme for two-dimensional Maxwell's equations in negative index metamaterials, J. Sci. Comput. 69 (2016) 696-735.
[37] T. Lu, P. Zhang, W. Cai, Discontinuous Galerkin methods for dispersive and lossy Maxwells equations and PML boundary conditions, J. Comput. Phys. 200 (2004) 549–580.
[38] P. Monk, Finite Element Methods for Maxwell's Equations. Oxford University Press, 2003.
[39] S. Nicaise and J. Venel, A posteriori error estimates for a finite element approximation of transmission problems with sign changing coefficients, J. Comput. Appl. Math. 235 (2011) 4272-4282.
[40] J.B. Pendry, D. Schurig and D.R. Smith, Controlling electromagnetic fields, Science 312 (2006). 1780-1782.
[41] A. Quarteroni, and V. Alberto, Numerical approximation of partial differential equations. Springer Ser, Comput. Math. 23, 2008.
[42] W.H. Reed and T.R. Hill, Triangular mesh methods for the neutron transport equation. Tech. Report LA-UR-73-479, Los Alamos Scientific Laboratory, 1973.
[43] C. Shi, J. Li and C.-W. Shu, Discontinuous Galerkin methods for Maxwell's equations in Drude metamaterials on unstructured meshes,J. Appl. Math. 342 (2018) 147-163.
[44] J. Wang, Z. Xie and C. Chen, Implicit DG method for time domain maxwell's equations involving metamaterials, Adv. Appl. Math. Mech. 7 (2015) 796-817.
[45] Y. Xu and C.-W. Shu, Local discontinuous Galerkin methods for high-order time-dependent partial differential equations, Commun. Comput. Phys. 7 (2010) 1-46.
[46] Z. Yang, L.-L. Wang, Z. Rong, B. Wang and B. Zhang, Seamless integration of global Dirichlet-to-Neumann boundary condition and spectral elements for transformation electromagnetics, Comput. Methods Appl. Mech. Engrg. 301 (2016) 137-163.

[47] S. Zhang, C.G. Xia and N. Fang, Broadband acoustic cloak for ultrasound waves, Phys. Rev. Lett. 106 (2011) 024301.